Monthly Scientific-Technical and Production Journal

The Paton WELDING JOURNAL

February 2001 # 2

English translation of the monthly «Avtomaticheskaya Svarka» journal published in Russian since 1948

The National Academy of Sciences of Ukraine
The E.O. Paton Electric Welding Institute of the NAS of Ukraine
International Association «Welding»

«The Paton Welding Journal»
is published monthly by the
International Association «Welding»

Promotion group:
V.N.Lipodaev, V.I.Lokteva
A.T.Zelnichenko (Exec. director)
Translators:
S.A.Fomina, I.N.Kutianova,
T.K.Vasilenko

Editorial and advertising offices
are located at PWI,
International Association «Welding»,
11, Bozhenko str., 03680,
Kyiv, Ukraine
Tel.: (38044) 227 67 57
Fax: (38044) 268 04 86
E-mail: tomik@mac.relc.com
E-mail: office@paton.kiev.ua

State Registration Certificate
KV 4790 of 09.01.2001

Subscriptions:
$460, 12 issues, postage included

«The Paton Welding Journal» Website:
http://www.nas.gov.ua/pwj

CONTENTS

MODERN ELECTRON BEAM TECHNOLOGIES OF THE E.O. PATON ELECTRIC WELDING INSTITUTE OF THE NAS OF UKRAINE

B.E. PATON
The E.O. Paton Electric Welding Institute, NASU, Kyiv, Ukraine

ABSTRACT

Technologies and equipment for EBW, electron beam vapour phase deposition and electron beam melting of titanium from a dispersed melt are described. Advantages of the technologies and examples of their application are considered.

Key words: *electron beam technologies, welding, melting, spraying, vapour phase deposition, condensed materials, refining*

Electron beam technologies (EBT) is a collective term, covering a number of efficient processes of production, treatment and welding of materials that have developed into yet another independent science and technology field over the last 40 years and are closely related to the progress of vacuum engineering and electron optics.

Broad prospects for automatic, and over the last years also computerised control of EBT, conducting in vacuum the processes that provide not only preservation of the initial purity of the processed material, but also its refining, high energy density in the electron beam, unachievable with the traditional heat sources — all this promotes EBT application both in the industries related to production of small-sized items (in instrument-making, electronics), and those manufacturing large-sized items (in heavy and power engineering, foundry, ship- and rocket-building).

In EBT the energy carrier is a powerful electron beam that makes an impact on the material being processed. The beam is generated in an electron beam gun where emission of free electrons, their acceleration in an electrostatic field, focusing and deflection of the beam by electromagnetic field, take place. The beam is taken into the working chamber through the gun orifice. The objects of the electron beam process, namely billets or materials, are placed into the chamber, or are loaded into it. During melting the material to be remelted is fed under the beam, and the molten material flows into the intermediate crucible or mould. In vapour deposition, devices for fastening, displacement and preheating of the items on the surface of which the evaporation material is deposited, are mounted in the working chamber in addition to the devices for feeding the evaporation material. In welding the item is placed into the chamber or fed into it continuously or piece by piece. The applied devices are highly specific, depending on the concrete purpose and largely determine the appearance of the unit as a whole.

The E.O. Paton Electric Welding Institute began development of EBT, in particular the technology and equipment for EBW, in 1958. The first laboratory unit for EBW was developed at that time.

Vacuum, accelerated electron beams, metal physics and metals science are the key fields of knowledge that determined the initial selection and further formation of the team of experts who are still working in the three main areas of EBT, namely welding, melting and vapour deposition. PWI is the world leader in each of these areas. This is confirmed by numerous patents, setting up and successful running of joint ventures and science and technology centers with participation of foreign partners, development and sale of equipment, technologies and know-how under foreign contracts.

EBT also has an important role in PWI activity as a whole. Three major research departments (about 150 staff scientists) are working completely in the above areas. The results of some recent research and development are given below for each of these areas.

Electron beam welding. Over the last 10 years the main areas of our work have been as follows:

- development of the technology and technique of single-pass EBW of large-sized items with the wall thickness of up to 250 mm (structural steels) and 400 mm (aluminium and titanium alloys);
- fabrication of production equipment for EBW.

Selection of the above areas of the Institute's activity was largely determined by the desire to enter the world market of EBW technologies and equipment in which a tough competition is created by such well-known companies as Steigerwald Schtrahltechnik (Germany), Sciaky (USA), Cambridge Vacuum Engineering (Great Britain) and Techmeta (France).

In the area of EBW of 250 – 400 mm thick metal we managed to become the world leader owing to an integrated approach, both in terms of equipment and technology, to solving this problem. In particular, development of powerful highly stable power units with quick-response control systems and electronic protection from breakdowns in the welding gun [1]

ensured formation of stable penetration of reproducible geometrical dimensions. Investigation of physico-metallurgical processes in the weld pool resulted in development of the methods to improve its stability and, thus, prevent defects in the cast zone (pores, lacks-of-fusion, peaks in the root part, and hot cracks in the weld middle part) [2]. Technology of EBW of low-alloyed steels, including circumferential welds up to 150 mm thick, with their defect-free closure, has been successfully implemented in production conditions. EBW has been many times applied in fabrication of structures of titanium and aluminium alloys up to 300 mm thick (Figure 1).

In addition, successful introduction into production of EBW of sheet metal should be also noted, in particular of a continuous bimetal blank for manufacturing machine band saws. A production line for this technology, set up in the Chinese-Ukrainian PATON-GLEZI Joint Venture, has already been in operation for two years in Shanghai [3].

Over the last years, we have complemented the parameter range of power units for EBW, produced in co-operation with SELMI (Sumy) (Table 1). Such a production of self-sufficient power units that actually are the soul of electron beam units, does not yet exist anywhere else in the world. This is exactly what gave us certain advantages in the world market.

The produced power units are fitted with the systems of computer control, diagnostics of the condition and making protocols of welding results (diagnostics results can be also transmitted by fax or e-mail from the user to the manufacturer for taking a prompt decision in case of a malfunction in the power unit systems), which further enhanced the competitiveness of our developments in the external market.

The capabilities of computer diagnostics can be best illustrated in the case of determination of the focal position and energy density of the beam. These are exactly the two parameters of the beam that characterise the weld geometry.

In order to perform the beam diagnostics operation, the operator of the EBW unit gives a command for automatic displacement of the welding gun into the beam diagnostics position. The gun is positioned opposite a massive target, on which an electron beam of maximal power can be aimed. A tungsten plate, grounded through a measuring resistor, is placed above the target, in the immediate vicinity of the electron beam. If the electron beam is momentarily deflected to this plate, a current pulse is generated in its circuit, the duration of the leading front of this pulse being inversely proportional to the density of electrons in the beam: the sharper the beam, the faster the current rise in the plate circuit. Having taken, for instance, 50 beam measurements at 50 different values of focusing current, we derive a pattern of the current density distribution along the beam length and can determine the position of the minimal beam diameter with an accuracy of ± 1 mm.

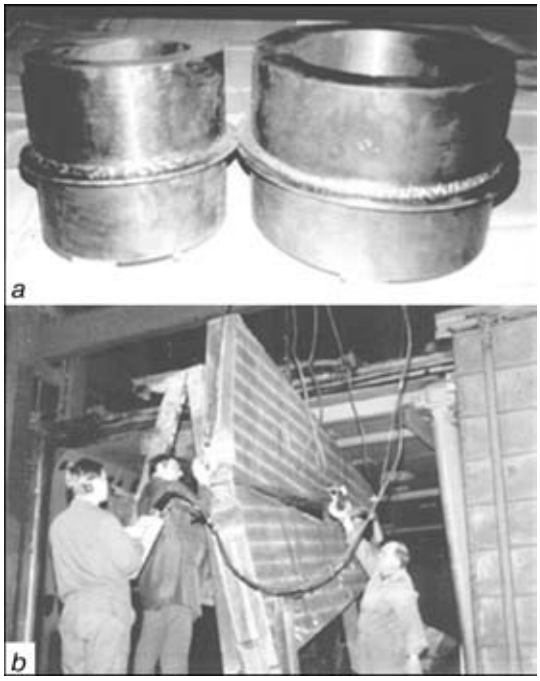

Figure 1. EB-welded thick-walled structures of low-alloyed steels (*a*) and aluminum alloy (*b*)

The entire process of beam diagnostics takes about 1 min, its result being a display showing longitudinal beam sections: top — initial (with a new cathode) and bottom — at a given moment of time. In the case, if cathode wear resulted in a change of the focal distance or reduction of the specific energy density in the electron beam, the diagnostic system will re-

Table 1. Parameter series of power units for EBW, produced by PWI and SELMI

Parameter	*ELA-3*	*ELA-15*	*ELA-30V*	*ELA-30/45*	*ELA-60*	*ELA-120/6*	*ELA-120V*
Beam power, kW	3	15	30	45	60	6	120
Accelerating voltage, kV	60	60	60	30	60	120	120
Set power, kV·A	5	25	57	70	90	8	220
Maximal weld depth, mm, in welding of							
steels	10	50	75	Melting and evaporation	100	15	250
titanium alloys	15	80	110		150	20	400
aluminium alloys	20	120	150		200	35	450

Notes: 1. Stability of accelerating voltage and beam current was ± 0.5 %. 2. Angle of beam deflection was ± 7°. 3. All power units are computer controlled.

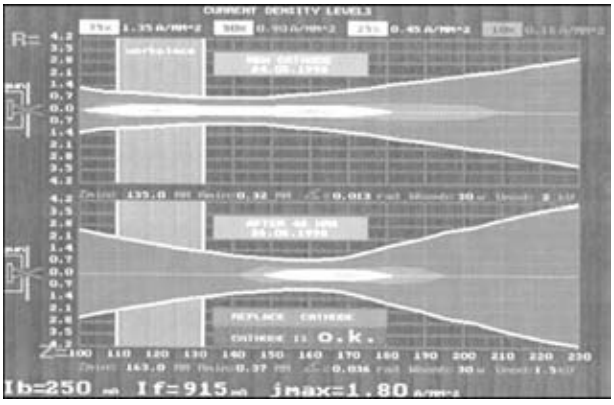

Figure 2. Computer display showing longitudinal sections of welding electron beams formed by a new cathode (*top*) and cathode after 48 h of operation (*bottom*), with the requirement to «Replace cathode»

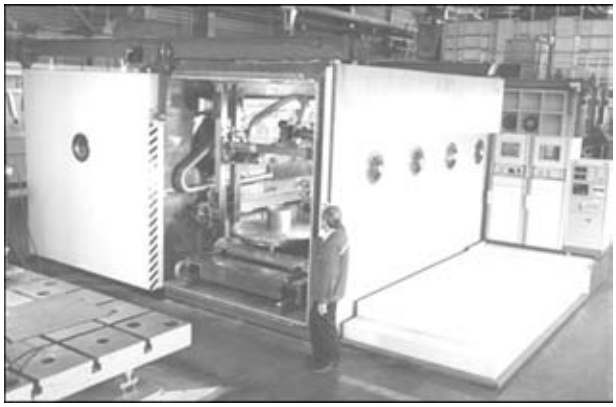

Figure 3. General view of a typical production unit of a new generation with a vacuum chamber of 2.5 × 2.5 × 5.0 m size for EBW of large-sized items

quire the operator to replace the worn cathode by a new one (Figure 2).

Figure 3 is a general view of a typical electron beam unit of a new generation for welding large-sized items. Units of this type have a modular design, consisting of a chamber, vacuum system and power unit. They can be both all-purpose and highly specialised. Their features are as follows:

- application of vacuum equipment produced by leading West European companies, in particular low-noise, reliable in operation mechanical pumps with a low oil ejection;
- use of linear guides in the modules of displacement of the welding gun and the item, thus allowing the accuracy of displacement and positioning to be raised up to the level of ± 0.1 mm.

Despite the application of relatively expensive components, the price of our equipment is by 30 % (for small-sized units) and 80 – 100 % (for large-sized units) lower compared to the foreign analogs.

Technology of electron beam physical vapour deposition (EBPVD) of materials. Investigations of physico-chemical processes of electron beam evaporation and subsequent condensation of different substances under vacuum began at PWI simultaneously with the work on EBW. The potential of these processes in terms of materials science had already been demonstrated by this time for the case of thin films.

The processes of evaporation and subsequent condensation of various substances, form a unique technological complex, allowing new materials to be developed. The point is that being in the vapour phase, the substances «do not know» the laws of solubility. Therefore, evaporating several substances simultaneously, mixing their vapour flows, and then condensing them on the substrate, it is possible to produce such combinations and ratios of components, create such structures that are very difficult or impossible to achieve by other methods.

The main purpose of research and development performed in the PWI, was developing the scientific principles and technologies and making electron beam equipment to produce massive (thick film) inorganic materials with special structure and properties.

Already by the middle of 1960s the technical means for high-speed evaporation of substances under vacuum were developed on the basis of powerful electron beam guns created by PWI, and systematic investigation of the structure and properties of massive condensates 1 – 2 mm thick was begun. Extensive experimental data accumulated by now, confirm the ability to produce from the vapour phase new inorganic materials with the specified composition and structure, also amorphous and fine-crystalline materials with a non-equilibrium structure, including diamondlike carbon-base phases; dispersion-strengthened, microlaminate and microporous materials based on metals, alloys and ceramics. It is also possible to synthesise on the condensation surface intermetallics, carbides, silicides and other refractory compounds, as well as multiphase systems on their base [4 – 6].

At present the technologies of evaporation and subsequent condensation of substances under vacuum can be regarded as a small, but independent field of vapour phase metallurgy. Figure 4 shows the growth of world production of metallic materials by the regular large-scale metallurgy (about $1 \cdot 10^9$ t/year), powder metallurgy (about $1 \cdot 10^6$ t/year), as well as vacuum evaporation and condensation (about $1 \cdot 10^3$ t/year). Despite a relatively small amount of metallic materials condensed from the vapour phase, their importance in the modern industrialised society is comparable with that of the traditional materials. It can be anticipated that their world production will grow up to $1 \cdot 10^4$ t/year in the next 15 years.

The productivity of modern electron beam evaporators, consisting of 3 – 4 sources (crucibles) is 10 – 15 kg of vapour per hour. The achieved maximal rates of condensation of the metals and alloys, are equal to 50 – 100 μm/min.

It is typical that the evaporation and condensation processes allow the material deposition on the substrate to be combined with some other technological requirements. For instance, the condensed material can be given the sought shape by deposition of the vapour flow on a surface of a specified configuration. Controlling the condensate bonding with the substrate allows achieving a good physical contact (ad-

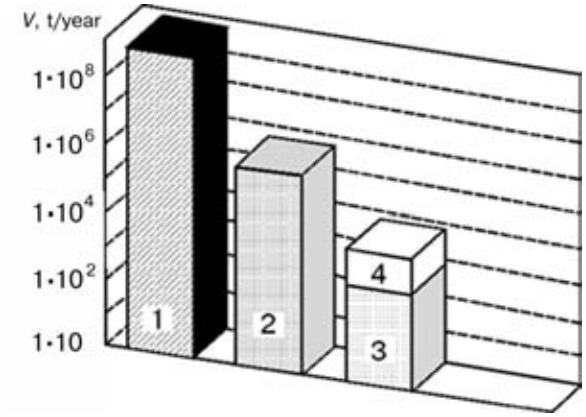

Figure 4. Volume of world production of metallic materials: *1* — traditional metallurgy; *2* — powder metallurgy; *3* — PVD; *4* — 2010 year forecast

hesion) on the interface, or, contrarily, creating the conditions for the produced material separation from the substrate.

The condensed materials can be produced in the following form: relatively thin (10 – 150 μm) coatings on finished items; thick (1 – 2 mm) structural coatings, fulfilling the function of a load-carrying element of structures; semi-finished products (foil, strip, sheet) in the form of blanks and items of a complex shape, for instance, bodies of revolution; massive (20 – 50 kg) billets for subsequent thermoplastic processing and forming them as required. It should be further noted that the processes of evaporation and condensation conducted under vacuum ($1 \cdot 10^{-3}$ – $1 \cdot 10^{-2}$ Pa) are perfect in terms of ecology, as they practically generate no harmful evolutions into the environment.

Figure 5 is a schematic representation of the structures of inorganic materials and coatings, produced by EBPVD. These materials are used in practice primarily in the form of various coatings, including high-temperature and corrosion-resistant, thermal barrier, super hard, wear-resistant, biocompatible coatings those with special electrical, magnetic and chemical properties, and for materials joining. The leading coatings now are protective coatings for gas turbine blades of various purposes, namely high-temperature and corrosion-resistant and, especially, thermal barrier coatings with an outer ceramic layer of zirconia.

Simultaneously with investigation of physico-chemical processes of evaporation and condensation, development of specific technologies of PVD of inorganic materials and coatings, PWI scientists continue development and further improvement of laboratory, pilot-production and production electron beam equipment for the above purposes.

Over the period of 1975 – 1985 the E.O. Paton Institute Pilot Plant made more than 15 production electron beam units designed for deposition of protective coatings on the blades of gas turbines for various purposes and mounted in the enterprises of aircraft-making and ship-building industry, as well as gas industry.

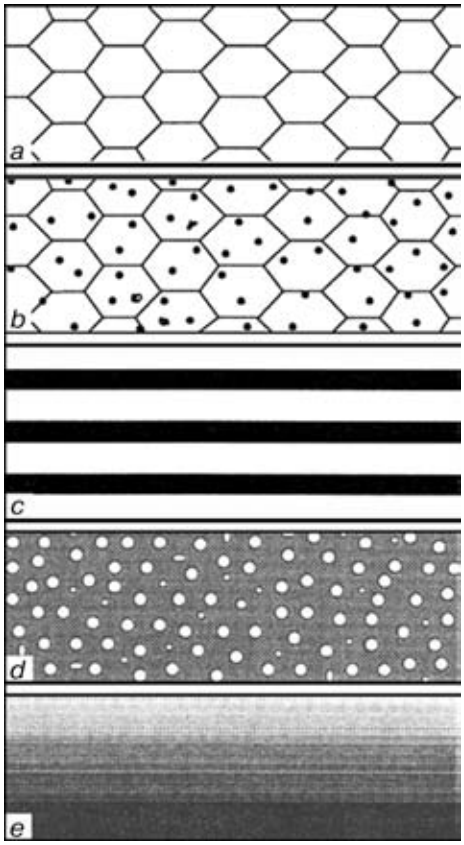

Figure 5. Structures of materials and coatings produced by EBPVD methods: *a* — single-phase; *b* — two-phase; *c* — microlaminate; *d* — microporous; *e* — gradient

New priority areas of PWI research and development currently are:

- functionally-graded thermal-barrier coatings for gas turbine blades, produced by evaporation of the composite ingot from one source;
- functionally-graded high-temperature, corrosion and erosion-resistant coatings, as well as hard coatings, deposited from one source, on the parts of power generation, chemical equipment and tools.

Figure 6 is the microstructure of the gradient thermal barrier coating on Rene-5 type alloy with the characteristic columnar structure in the outer ceramic layer. The coating was produced by evaporation of a composite metal-ceramic ingot from one source. The thickness of the outer ceramic layer is 120 – 150 μm.

Over the recent period some advanced materials, used for scientific purposes in the form of items, sheets, foil or coatings, for instance, targets of intermetallics and silicides for magnetron sputtering; foil of shape-memory alloys (NiTi, etc.); coatings of alloys with a quasi-crystalline structure, have been produced at PWI.

PWI continues making laboratory and production electron beam equipment and conducting specialist training.

In the field of EBPVD, PWI co-operates with success with companies and scientific centers from USA, Europe and Asia.

Advanced EBT of melting titanium and producing composite materials by melt dispersion. Devel-

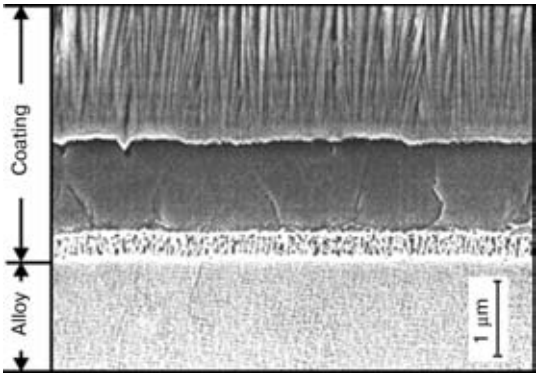

Figure 6. Mictrostructure of a gradient thermal barrier coating on Rene-5 type alloy

Figure 7. Slab ingots of VT1-00 alloy of 160 × 950 × 2000 mm size produced by EBMIC process

opment of the technology and production equipment to implement the electrometallurgical process of making sound high-quality ingots of titanium and its alloys from titanium sponge and wastes, by the method of electron beam melting with an intermediate crucible (EBMIC) without any preliminary pressing of the consumable electrodes, has evolved into an independent area of PWI activity [7, 8]. The above technology allows production of ingots of both round (150 – 840 mm in diameter) and rectangular (160 × × 950 mm) cross-section of up to 2200 mm length and subsequent electron beam melting of their side surface to eliminate mechanical treatment (stripping, turning, abrasive treatment) before further processing. It results in saving up to 15 % of the metal and lowering labour expenses by up to 35 %.

Ability to produce slab ingots of a rectangular cross-section (Figure 7) allows lowering the cost of plates production, as it eliminates from the technological sequence, the operation of forging cylindrical ingots into slabs and their subsequent machining, thus increasing the yield.

Use of an intermediate crucible enables refining the metal from alpha-particles. The technology provides the stability and uniformity of the composition, high quality of ingots from Ti-based alloys, as well as the content of easily evaporating aluminium in the ingot within the requirements of the standards (Table 2).

It is known that a great hazard is constituted by entrapment in the ingot of refractory inclusions of titanium sponge, saturated mainly with nitrogen, that later on can lead to unexpected failure of the structure. EBMIC is exactly the radical method for removal of such inclusions during the ingots melting. During the time of the liquid metal staying in the intermediate crucible, the heavy (with more than 4 g/cm^3 density) particles go to the bottom and accumulate in the skull, while lighter elements (with the density below 4 g/cm^3), float to the melt surface where they are destroyed under the impact of the electron beam.

It should be emphasized once more that unlike the existing concepts of electron beam melting being applicable just for processing titanium wastes, or, at the most, producing commercial titanium ingots, our technology allows making ingots of complex titanium alloys by remelting titanium sponge and master alloy [7, 8].

By the use of less expensive initial material (titanium sponge of TG-130 grade) and increasing the efficient metal yield, EBMIC allows lowering the cost of titanium semi-finished products and, therefore, expanding the areas of titanium application in different industries. PWI has a production shop for electron beam melting (Figure 8), the capacity of which allows production of commercial batches of titanium ingots

Table 2. Content of alloying and impurity elements in titanium ingots produced by EBMIC process

Alloy grade	*Sample location*	*Content of elements, wt.%*							
		Al	*V*	*C*	*Fe*	*Si*	*O*	*N*	*H*
VT6	Top	5.90	4.38	0.01	0.08	0.02	0.08	0.02	0.001
	Middle	6.00	4.30	0.02	0.10	0.02	0.08	0.02	0.001
	Bottom	6.00	4.38	0.01	0.09	0.03	0.08	0.02	0.001
GOST 19807–74		5.30 – 6.80	3.50 – 5.30	0.10	0.30	0.15	0.20	0.05	0.015
VT1-00	Top	0.27	–	0.03	0.08	0.04	0.07	0.02	0.001
	Middle	0.30	–	0.02	0.10	0.02	0.06	0.02	0.001
	Bottom	0.24	–	0.02	0.12	0.03	0.07	0.03	0.001
GOST 19807–74		0.30	–	0.05	0.20	0.08	0.10	0.04	0.008

Figure 8. General view of the shop for electron beam melting of titanium ingots

of various type sizes with the annual output of up to 1500 t.

Composite materials are finding ever wider application in different industries lately. One of the new processes of development of composite materials of metal–ceramics type, as well as metal–metal type, is EBT for producing structural materials from a dispersed melt.

The essence of the process consists in melting with the electron beam a consumable billet that rotates at a high speed (about 1500 rpm), forming a directed flow of a dispersed melt at the expense of the centrifugal forces, its layer-by-layer deposition on the forming surface or on a reinforcing filler with formation of a composite billet or coating of specified geometrical dimensions and shape.

The technology has the following features:

- use of vacuum to provide the purity of both the materials proper, and the surfaces being joined, prevention of microporosity in the materials related to collapse of gas bubbles;
- melting of the consumable billet with the electron beam that allows variation of the drop dimensions and density of the dispersed melt flow in a wide range;
- dosed heating of the substrate thus guaranteeing a strong bonding of the dispersed melt with the substrate and high density of the precipitate;
- ample possibilities for stabilizing the parameters and automatic control of the technological process.

PWI developed and made specialized technological equipment based on UE-121 electron beam unit, that allows making, with up to 300 kg/h efficiency, composite blanks and semi-finished products of up to 200 kg weight of a configuration close to that of the finished item (Figure 9), restoring worn parts, producing coatings with specified physico-chemical properties, and welding difficult-to-weld materials without melting the edges. This process enables joining materials that cannot be joined by the traditional technologies. So, for instance, alumina ceramic tiles are joined by aluminium melt. Joint strength higher than that of the ceramic component is achieved. Bimetal steel–titanium tubular billets have been made, with 150 MPa strength of the metal joint.

Figure 9. Billet for the die of a complex-shaped extruder

The method is especially effective for production of billets and semi-finished products of complex alloys based on aluminium, nickel, titanium, as well as refractory metals.

In conclusion in should be noted that EBT of materials melting and processing rightfully belong to the highest level of technologies offering great prospects and having highly effective application.

REFERENCES

1. Paton, B.E., Nazarenko, O.K. (1989) *Electron beam welding: achievements and problems (Review)*. Hardwood: Academic Publ.
2. Nesterenkov, V.M., Nazarenko, O.K., Akopyants, K.S. (1998) Closing of circumferential welds of thick steels. In: *Proc. of 6th Int. Conf. on Welding and Melting by Electron and Laser Beam*, Toulon, June 15 – 19.
3. Nazarenko, O.K., Orsa, Yu.V., Stoliko, Yu.Ya. (2001) Prospects for electron beam welding in fabrication of bimetal band saws and saw blades in Ukraine. *Avtomaticheskaya Svarka*, **1**, 26 – 32.
4. Paton, B.E., Movchan, B.A. (1991) Composite materials deposited from the vapour phase in vacuum. Soviet Technologies Reviews. *Welding and Surfacing Reviews*, **2**, 43 – 64.
5. Paton, B.E., Movchan, B.A., Osokin, V.A. *et al*. (1994) Electron beam technology of producing and mechanical properties of thick Al and Al–ZrB_2 condensates. *Problemy Spets. Elektrometallurgii*, **1/2**, 33 – 37.
6. Movchan, B.A. (1998) Inorganic materials deposited from the vapour phase under vacuum. In: *Modern Material Science. XXI century*. Kyiv: Naukova Dumka.
7. Paton, B.E., Trigub, N.P., Akhonin, S.V. *et al*. (1996) Some tendencies in development of metallurgical processing of titanium. *Problemy Spets. Elektrometallurgii*, **1**, 25 – 31.
8. Paton, B.E., Trigub, N.P., Akhonin, S.V. (2000) Electron beam melting of titanium. In: *Proc. of 9th Int. Conf. on Titanium*, S.-Petersburg, June 7 – 11, 1999. Prometej Inst.

ASSESSMENT OF FATIGUE LIFE OF TUBULAR CONNECTIONS SUBJECTED TO ULTRASONIC PEENING TREATMENT*

E.F. GARF[1], **A.E. LITVINENKO**[1] and **A.Kh. SMIRNOV**[2]
[1]The E.O. Paton Electric Welding Institute, NASU, Kyiv, Ukraine
[2]I.M. Gubkin State Academy of Oil and Gas, Moscow, Russia

ABSTRACT

Feasibility of extension of life of operating welded structures, made from tubes, by using the peening treatment of the zone of welding is considered. It is shown that the use of a linear hypothesis of accumulation of the fatigue damage is rightful for the estimation of the full life. Moreover, the peening treatment of welded joints increases the material fatigue strength.

Key words: *ultrasonic peening treatment, welded joint, tubular connections, fatigue resistance, fatigue life, life, residual life, fatigue testing*

In case of optimal design of latticed tubular structures, a lot of attention should be given to connection strength [1, 2], and, primarily, in structures exposed to cyclic loading in addition to static loads in service. Features of stress-strain state in the tubular connection zone consist in that a higher stress concentration is found at the welded joint boundary, related not only to the presence of the weld, but also to the mode of force transfer in the connected cylindrical shells. Stress distribution in the weld zone is markedly nonuniform both around the welded joint perimeter, and across the wall thickness of the connection elements. Stress gradients, as well as the areas with maximal levels of stress concentration [3] depend on connection type and loading mode.

Fatigue resistance of tubular truss structures is determined by fatigue resistance of welded connections. Therefore, increase of fatigue resistance of tubular connections, is an effective method of lowering the metal content of structures and extension of their life. Ultrasonic peening treatment of the welded joint zone (UPTWJZ), probably, is one of the most promising methods for improvement of fatigue resistance of tubular connections [4 – 9].

Procedures for fatigue analysis of tubular connections with welded joints in the initial condition and especially, after UPTWJZ [10], have been developed over the last years. On the other hand, a considerable number of tubular structures were designed at the time when the issues of connection strength (and primarily, under cyclic loading), were insufficiently studied, and the procedures for their fatigue analysis were absent. The design life of these structures is almost over, and, therefore, the issue of extension of their service life is extremely urgent. In this connection, use of UPTWJZ to improve the fatigue life of welded connections of tubular structures in service, is a quite promising method.

This paper deals with an approach to evaluation of residual life of tubular structures after UPTWJZ performed during the structure service, i.e. those having a certain level of fatigue damage accumulation in the initial condition after welding by the moment of treatment performance.

The proposed procedure for residual life evaluation, is based on the results of fatigue testing of full-scale tubular connections (Figure 1) of steel 20 (C — 0.17 – 0.24; Mn — 0.35 – 0.63; Si — 0.17 – 0.37; S — up to 0.04 wt.%) with the yield point of 299 – 333 MPa, and ultimate strength of 410 – 493 MPa. Joints were welded manually with complete penetration with UONI-13/55 (C — 0.09; Mn — 0.9; Si — 0.43; S — 0.03; P — 0.03 wt.%) electrodes of 3 mm (root weld) and 4 mm diameter. The weld leg was ~8 mm.

Fatigue testing was conducted in two stages. In the first stage, it was performed in the initial condition after welding to achieve accumulation of fatigue damage to the level equal to 0.25 – 0.60 of that leading to fatigue crack initiation and was stopped after that. This was followed by UPTWJZ. In the second stage, testing of connections after UPTWJZ was continued up to initiation of the fatigue macrocrack at $5 \cdot 10^6$ loading cycles. Testing was performed at a symmetrical cycle of connections loading by in-plane bending moment. Ranges of effective stresses in the locations of the anticipated fatigue crack initiation (along the welded joint boundary from the side of the girth or brace) were calculated, and the number of loading cycles in each of the testing stages was recorded. Stress levels in the first and second testing stages can be different.

Proceeding from S–N curves derived in [9] for tubular connections in the initial condition and with

*Technology and equipment for performance of UPTWJZ were developed by GNPP «Kvant» (Severodvinsk, Russia) and E.O. Paton Electric Welding Institute.

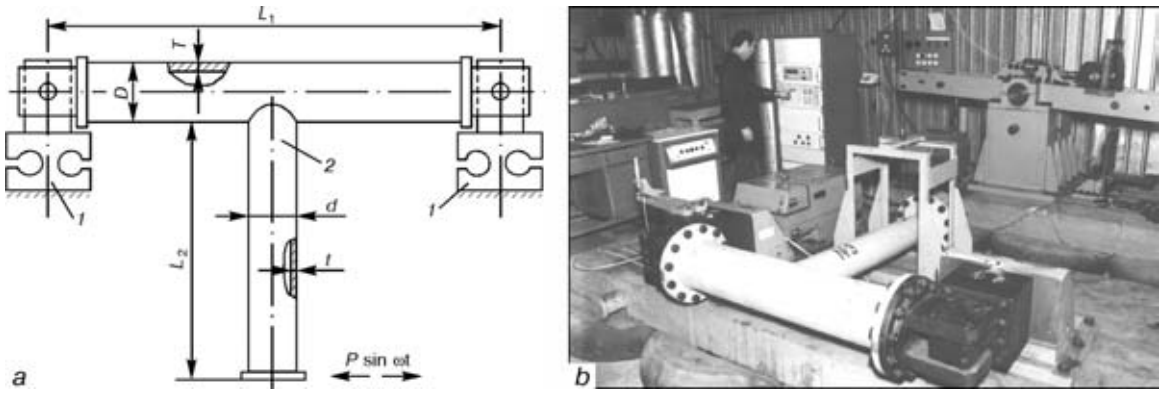

Figure 1. Fatigue testing of tubular T-shaped connections: *a* — sample schematic; *b* — testing facility; *1* — dynamometric supports; *2* — welded tubular T-shaped connection; L_1, L_2 — length of girth pipe and brace pipe, respectively; T, t — thickness of girth pipe and brace pipe, respectively; D, d — diameter of girth pipe and brace pipe, respectively

application of UPTWJZ, performed before the start of testing, the limit number of loading cycles and accumulation of fatigue damage were determined, for each connection in each of the testing stages and on the whole up to the macrocrack initiation, for the respective loading mode and fatigue crack initiation site, depending on the effective stress range.

Results of tubular connections testing are given in Table 1. The ratio of geometrical dimensions of elements in connections No.1 – 10 was taken to be such that the fatigue crack initiated in the girth, and in connections No.11 – 16 fracture occurred in the truss element. These data demonstrate that using the accepted testing procedure, achievement of the limit state (fatigue macrocrack initiation) corresponds to the total accumulation of fatigue damage ≈1.0, irrespective of the site of fatigue crack initiation (in the girth or the brace). In addition, if in the second stage of testing after UPTWJZ, the effective stress ranges were lower than the fatigue limit for the treated connections, no fatigue crack initiation was recorded. This conclusion is extremely important, as in the actual structures, fatigue damage accumulation is mostly found at low levels of cyclic stresses close to the fatigue limit. After UPTWJZ the fatigue limit is significantly increased and, therefore, low stress levels do not participate in fatigue damage accumulation. This, apparently, will be the main factor in improvement of fatigue life of tubular connections after UPTWJZ performed during the structure service.

Analysis of scatter of fatigue damage accumulation, corresponding to achievement of limit condition of welded connections, derived in fatigue testing, revealed the normal distribution law (Figure 2) with parameters of mathematical expectation $a = 1.064$ and

Table 1. Results of testing tubular connections loaded by in-plane bending moment

No.	Girth section, $D \times T$, mm	Brace section, $d \times t$, mm	Loading without treatment				Loading after treatment				Sum of accumulated fatigue damage, %
			$2\sigma_\alpha$, MPa	N_i, cycle	n_i, cycle	n_i/N_i, %	$2\sigma_\alpha$, MPa	N_j, cycle	n_j, cycle	n_j/N_j, %	
1	219.75 × 7.9	147.14 × 7.96	70.0	$1 \cdot 10^6$	$5.17 \cdot 10^5$	51.7	110.0	$1.53 \cdot 10^6$	$7.5 \cdot 10^5$	49.0	100.7
2	219.75 × 7.9	147.14 × 7.96	70.0	$1 \cdot 10^6$	$5.17 \cdot 10^5$	51.7	110.0	$1.53 \cdot 10^6$	$9.0 \cdot 10^5$	58.8	110.5
3	219.11 × 7.88	146.6 × 8.2	84.3	$5 \cdot 10^5$	$2.5 \cdot 10^5$	50.0	100.0	$3.212 \cdot 10^6$	$5.0 \cdot 10^6$	155.6	205.6
4	219.11 × 7.88	146.6 × 8.2	84.3	$5 \cdot 10^5$	$2.5 \cdot 10^5$	50.0	120.0	$7.77 \cdot 10^5$	$4.3 \cdot 10^5$	55.3	105.3
5	219.11 × 7.88	146.6 × 8.2	84.3	$5 \cdot 10^5$	$2.5 \cdot 10^5$	50.0	120.0	$7.77 \cdot 10^5$	$5.1 \cdot 10^5$	65.6	115.6
6	219.4 × 8.1	146.7 × 8.6	84.3	$5 \cdot 10^5$	$1.26 \cdot 10^5$	25.2	130.0	$4.17 \cdot 10^5$	$2.33 \cdot 10^5$	55.9	81.1
7	219.4 × 8.1	146.7 × 8.6	84.3	$5 \cdot 10^5$	$1.26 \cdot 10^5$	25.2	130.0	$4.17 \cdot 10^5$	$2.62 \cdot 10^5$	62.8	88.0
8	219.5 × 8.1	146.9 × 8.6	70.0	$1 \cdot 10^6$	$2.5 \cdot 10^5$	25.0	110.0	$1.53 \cdot 10^6$	$1.21 \cdot 10^6$	79.0	104.0
9	219.5 × 8.2	146.7 × 8.4	70.0	$1 \cdot 10^6$	$3.5 \cdot 10^5$	35.0	70.0	$5.16 \cdot 10^7$	$5.0 \cdot 10^6$	Did not break	
10	219.5 × 8.2	146.7 × 8.4	70.0	$1 \cdot 10^6$	$3.5 \cdot 10^5$	35.0	100.0	$3.212 \cdot 10^6$	$2.69 \cdot 10^6$	83.7	118.7
11	219.7 × 7.71	158.7 × 4.48	109.7	$1 \cdot 10^6$	$5 \cdot 10^5$	50.0	134.0	$1 \cdot 10^6$	$0.803 \cdot 10^6$	80.0	130.0
12	219.14 × 7.81	158.8 × 4.46	123.7	$5 \cdot 10^5$	$2.5 \cdot 10^5$	50.0	123.7	$1.79 \cdot 10^6$	$1.03 \cdot 10^6$	57.5	107.5
13	219.48 × 7.91	158.84 × 4.41	115.3	$7.5 \cdot 10^5$	$4 \cdot 10^5$	53.0	134.0	$1 \cdot 10^6$	$4.9 \cdot 10^5$	49.0	102.0
14	219.35 × 7.73	158.85 × 4.44	102.0	$1.5 \cdot 10^6$	$7.5 \cdot 10^5$	50.0	127.0	$1.5 \cdot 10^6$	$1.07 \cdot 10^6$	71.3	121.3
15	219.5 × 7.5	158.8 × 4.45	100.0	$1.7 \cdot 10^6$	$8 \cdot 10^5$	47.0	130.0	$1.26 \cdot 10^6$	$6.5 \cdot 10^5$	51.6	98.6
16	219.6 × 7.7	158.8 × 4.4	120.0	$6.12 \cdot 10^5$	$2.5 \cdot 10^5$	40.8	130.0	$1.26 \cdot 10^6$	$8.2 \cdot 10^5$	65.1	105.9

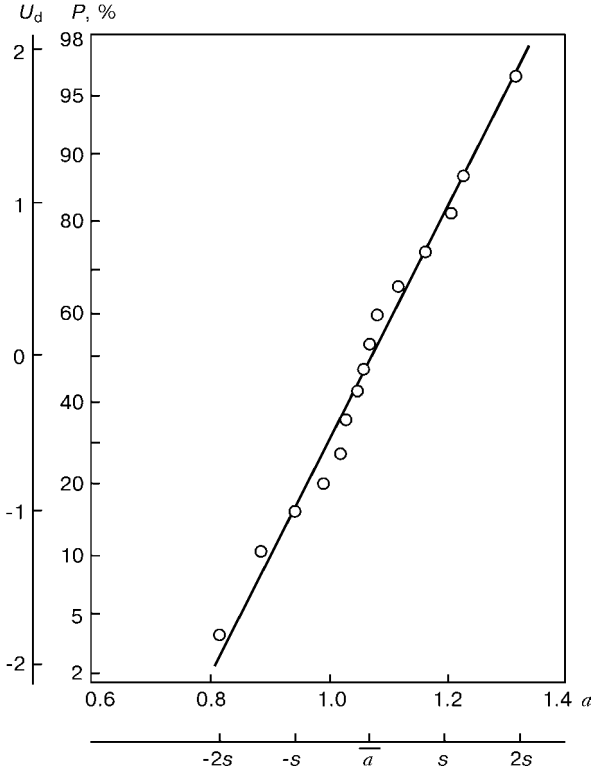

Figure 2. Distribution of fatigue damage accumulation in tubular connections when UPTWJZ is performed after fatigue damage accumulation in initial condition: U_d — quantile of normal distribution; P — failure probability; s — root mean square deviation

sample standard deviation $s = 0.128$, thus allowing the hypothesis of linear accumulation of fatigue damage to be used in development of the design procedure.

Experimentally-based statement of the validity of using the hypothesis of linear accumulation of fatigue damage, for evaluation of the limit condition of tubular connections in fatigue analysis, extended to the cyclic loading stage, both in as-welded condition and after UPTWJZ, can be represented in the following form:

$$a \le a_p, \quad a_p = \sum \frac{n_i}{N_i} + \sum \frac{n_j}{N_j} = 1.0,$$

where a, a_p are fatigue damage accumulation and limit accumulation of fatigue damage, respectively; n_i is the number of loading cycles with the effective stress range of $2\sigma_{\alpha i}$ during the period of the connection service in as-welded condition; N_i is the limit number of loading cycles under the impact of cyclic stress ranges $2\sigma_{\alpha i}$ for connections in as-welded condition; n_j is the number of loading cycles with effective stress range $2\sigma_{\alpha j}$ over the planned period of connection service after UPTWJZ; N_j is the limit number of loading cycles under the impact of effective stress ranges $2\sigma_{\alpha j}$ for components after UPTWJZ performed before the start of loading.

Considering that in the actual tubular welded structures, the elements can be loaded by longitudinal force P, in-plane bending moment M_b and out-of-plane bending moment M_c and that depending on a combination of geometrical dimensions of elements, the crack can initiate in the welded joint zone either from the side of the girth, or from the side of the brace, while the S–N curves for each loading mode and type (site) of cyclic fracture are different, it is rational to introduce the notion of effective stresses equivalent in their damaging action. The latter are determined proceeding from the condition of reducing S–N curves to the basic curve, which was taken to be the curve for as-welded tubular connections when loaded by a longitudinal force and crack initiation in the girth.

Table 2 gives the earlier derived equations of S–N curves for tubular connections in as-welded condition and after UPTWJZ, performed before the start of cyclic loading. Values of coefficients B, b for determination of effective stresses $2\sigma_{\alpha e}$ equivalent in their damaging action, are also given in keeping with expression

$$2\sigma_{\alpha e} = B\,(2\sigma_{\alpha})^b.$$

Ranges of $2\sigma_{\alpha}$ in the welded joint zone from the side of the girth or the brace, depending on the connection design, geometrical parameters of the elements and kind of loading, are found from expressions given in [10].

In fatigue analysis of welded connections of tubular structures, the common method is using stress ranges as loading parameter. Such an approach does not allow for the influence of the loading cycle characteristic. Proceeding, however, from the high levels of stress concentration in tubular connections, the influence of the loading cycle characteristic is smaller than with other types of welded joints and it is usually ignored.

Table 2. Equations of S–N curves of welded tubular connections in the initial condition and after UPTWJZ

Loading mode	*Initial condition*			*After UPTWJZ*			*Fracture site*
	S–N curve equations	B_i	b_i	*S–N curve equations*	B_i	b_i	
N	$\lg N + 4.284 \lg 2\sigma_{\alpha} = 13.420$	1.0	1.0	$\lg N + 7.991 \lg 2\sigma_{\alpha} = 21.571$	$1.251 \cdot 10^{-2}$	1.865	Girth
M_b	$\lg N + 3.769 \lg 2\sigma_{\alpha} = 12.956$	1.283	0.88	$\lg N + 7.783 \lg 2\sigma_{\alpha} = 22.073$	$9.553 \cdot 10^{-3}$	1.817	
M_c	$\lg N + 9.244 \lg 2\sigma_{\alpha} = 22.457$	$7.78 \cdot 10^{-3}$	2.158	$\lg N + 10.918 \lg 2\sigma_{\alpha} = 26.267$	$1.003 \cdot 10^{-3}$	2.549	
N	$\lg N + 4.712 \lg 2\sigma_{\alpha} = 15.930$	0.26	1.1	$\lg N + 7.900 \lg 2\sigma_{\alpha} = 24.001$	$3.389 \cdot 10^{-3}$	1.844	Brace
M_b	$\lg N + 5.775 \lg 2\sigma_{\alpha} = 17.782$	$9.6 \cdot 10^{-2}$	1.35	$\lg N + 7.384 \lg 2\sigma_{\alpha} = 21.711$	$1.161 \cdot 10^{-2}$	1.725	
M_c	$\lg N + 6.025 \lg 2\sigma_{\alpha} = 19.247$	$4.37 \cdot 10^{-2}$	1.41	$\lg N + 7.435 \lg 2\sigma_{\alpha} = 22.815$	$6.411 \cdot 10^{-3}$	1.736	

In fatigue analysis of welded connections of tubular elements exposed to complex cyclic loading, when a longitudinal force and bending moments are simultaneously applied to the element, the range of effective stresses equivalent in their damaging action should be determined in a differentiated manner for each stage of the connection service (as-welded and after UPTWJZ), allowing for the zones of maximal levels of working stresses around the tubular connection perimeter, induced by a particular applied force and using the values of coefficients given in Table 2, according to the following expressions:

for the stage of structure service in as-welded condition and criteria of fatigue crack initiation:

a) in the girth element

$$2\sigma_{\alpha e} = 2\sigma^D_\alpha(N) + 1.283\ (2\sigma^D_\alpha(M_b))^{0.88},$$

$$2\sigma_{\alpha e} = 2\sigma^D_\alpha(N) + 7.78\cdot10^{-3}(2\sigma^D_\alpha(M_c))^{2.16};$$

b) in the truss element

$$2\sigma_{\alpha e} = 0.26(2\sigma^d_\alpha(N))^{1.1} + 9.59\cdot10^{-2}(2\sigma^d_\alpha(M_b))^{1.35},$$

$$2\sigma_{\alpha e} = 0.26(2\sigma^d_\alpha(N))^{1.1} + 4.36\cdot10^{-2}(2\sigma^d_\alpha(M_c))^{1.41};$$

for the stage of structure service after UPTWJZ and criteria of fatigue crack initiation:

a) in the girth element

$$2\sigma_{\alpha e} = 1.251\cdot10^{-2}(2\sigma^D_\alpha(N))^{1.865} + 9.553\cdot10^{-3}(2\sigma^D_\alpha(M_b))^{1.817},$$

$$2\sigma_{\alpha e} = 1.251\cdot10^{-2}(2\sigma^D_\alpha(N))^{1.865} + 1.003\cdot10^{-3}(2\sigma^D_\alpha(M_c))^{2.549};$$

b) in the truss element

$$2\sigma_{\alpha e} = 3.389\cdot10^{-3}(2\sigma^d_\alpha(N))^{1.844} + 1.161\cdot10^{-2}(2\sigma^d_\alpha(M_b))^{1.725},$$

$$2\sigma_{\alpha e} = 3.389\cdot10^{-3}(2\sigma^d_\alpha(N))^{1.844} + 6.411\cdot10^{-3}(2\sigma^d_\alpha(M_c))^{1.736}.$$

In determination of fatigue damage accumulation or evaluation of a structure life, larger of the stress range values are used that have been derived by one of the above expressions for the appropriate stage of the connection service (as-welded or after treatment) and type of cyclic fracture (in the girth or the truss element).

Analysis of effectiveness of UTPWJZ, performed during the structure service, illustrated by the case of a connection of an off-shore platform, demonstrated that with the residual life of 2 years in as-welded condition, treatment allows extending the safe life up to 12 years.

CONCLUSIONS

1. Application of UPTWJZ is an effective method for extension of the life of connections of welded tubular truss structures exposed to cyclic loading in service, irrespective of the level of fatigue damage accumulation in the structure at the stage of its service in as-welded condition.

2. Extension of structure life by their UPTWJZ during service is, primarily, related to improvement of the fatigue limit.

3. Accumulation of fatigue damage in tubular connections after UPTWJZ performed after a certain period of structure service in the initial condition, is determined by their adding up at the stage of service in the initial condition and after treatment. Use of the hypothesis of linear accumulation of fatigue damage in fatigue analysis is valid.

REFERENCES

1. Marshall, P.W. (1984) Connections for welded tubular structures. In: *Proc. of 2nd Int. Conf. on Welding of Tubular Structures,* Boston, July 16 – 17. Boston: Pergamon Press.
2. Garf, E.F., Dyskin, E.M., Kazachek, V.M. (1997) Offshore platforms. In: *Welded structures for construction*. Kyiv: PWI.
3. Garf, E.F., Litvinenko, A.E. (1983) Influence of the angle of the brace meeting the girth on the strength of tubular welded connections loaded by bending moments. *Avtomaticheskaya Svarka*, **6**, 5 – 7.
4. Paton, B.E., Lobanov, L.M., Statnikov, E.Sh. *et al. A method of ultrasonic peening treatment and operational technological system for its implementation*. Pat. **12741** Ukraine, Int. Cl. 21 D 10/04. Publ. 28.02.97.
5. Mikheev, P.P. (1990) Improvement of fatigue resistance of welded joints in structures by ultrasonic peening treatment. In: *Transact. of PWI on Problems of Welding and Special Electrometallurgy*. Kyiv: Naukova Dumka.
6. Mikheev, P.P., Nedoseka, A.Ya., Parkhomenko, I.V. *et al.* (1984) Effectiveness of application of ultrasonic peening treatment to improve the fatigue resistance of welded joints. *Avtomaticheskaya Svarka*, **3**, 4 – 7.
7. Statnikov, E.Sh., Shevtsov, E.M., Kulikov, V.F. (1977) Ultrasonic peening tool for strengthening the welds and reducing residual stresses. In: *New physical methods of technological processes intensification*. Moscow: Metallurgia.
8. Mikheev, P.P., Garf, E.F., Kuzmenko, A.Z. *et al.* (1992) Improvement of fatigue resistance of tubular welded connections by ultrasonic peening treatment. *Avtomaticheskaya Svarka*, **11/12**, 3 – 6.
9. Mikheev, P.P., Garf, E.F., Kuzmenko, A.Z. *et al.* (1966) Improvement of fatigue resistance of tubular welded connections by ultrasonic peening. *Int. J. Off-shore and Polar Eng.*, **4**, 304 – 308.
10. Garf, E.F. (1995) Fatigue analysis of tubular welded connections after ultrasonic peening treatment. *Avtomaticheskaya Svarka*, **9**, 24 – 27.

FORMATION OF EMBRITTLED LAYERS ON TITANIUM AT ITS INTERACTION WITH STEEL TECHNOLOGICAL FIXTURE UNDER THE CONDITIONS OF DIFFUSION BONDING

V.V. SHURUPOV[1], **V.V. PESHKOV**[1], **M.N. SHUSHPANOV**[1] and **L.S. KIREEV**[2]
[1]Voronezh Aircraft Stock Society, Voronezh, Russia
[2]The E.O. Paton Electric Welding Institute, NASU, Kyiv, Ukraine

ABSTRACT

In diffusion bonding, the embrittled diffusion layers are formed at the titanium alloy surface as a result of a contact interaction of VT6 alloy products with a steel technological fixture. In contact with steel 12Kh18N10T the process of formation of embrittled layers is controlled by a heterodiffusion of steel components in the diffusion zone, containing intermetallics, while in contact with steel 20 — by carbon diffusion in the carbide-containing layer, interlocking iron diffusion into titanium.

Key words: *diffusion bonding, technological fixture, embrittled layer, contact interaction, intermetallics*

Fabrication of titanium large-sized thin-walled structures for the aircraft and aerospace engineering using a diffusion bonding is a promising trend in the welding industry [1]. When the technology of such processes is developed, a special attention is paid to the assurance of strength of a welded joint of a load-carrying skin with a filler [1]. However, the quality of the welded structure, a fatigue life and corrosion resistance in particular, are determined not only by the strength of the diffusion bonding, but also by the condition of surfaces and near-surface layers of the load-carrying skins which influence their service characteristics.

Under the conditions of the diffusion bonding, the diffusion processes together with an adhesion [2] can be developed between the surfaces of load-carrying skins and a fixture (technological sheets providing the transfer of the welding pressure to the workpiece), leading to the formation of new phases, chemical compounds, solid solutions, etc.

The preliminary investigations showed that the surface part of diffusion layers, formed on titanium under the conditions of its contact interaction with steel, is characterized by a low resistance to initiation of cracks and can be easily subjected to a brittle fracture at the applied stress.

To recover the ductile properties of the titanium surface after such interaction, an information about the thickness of formed embrittled layers is required. Therefore, the present work was aimed at the study of kinetics of formation of diffusion layers on titanium at its interaction with steels of different chemical composition under the diffusion bonding conditions.

Experiments were performed on samples of titanium alloy VT6 (Al — 5.3 – 6.8; V — 3.5 – 5.3 wt.%), used for the load-carrying skins, and also steels 20 (C — 0.17 – 0.24; Mn — 0.35 – 0.63; Si — 0.17 – 0.37; S — up to 0.04 wt.%) and 12Kh18N10T (C — ≤ 0.12; Cr — 17.0 – 19.0; Ni — 9.0 – 11.0; Si — ≤ 0.8; Mn — 1.0 – 2.0; S — up to 0.02; P — up to 0.035 wt.%), from which the technological sheets were made. In titanium interaction with these steels, both the processes, accompanied by the formation of chemical compounds (carbides, intermetallics), and also the mutual diffusion of iron and titanium, accompanied by the diffusion of chromium and nickel into titanium, can be developed [3].

Each of steel components (iron, carbon, chromium, nickel) cannot cause the essential changes in properties of titanium, but their complex action on the latter can be accompanied by decrease in its resistance to cracking and embrittlement. Therefore, even such method of examination as X-ray microanalysis which gives information about element composition of the metal, cannot reveal the presence and size of the most hazardous embrittled part of the diffusion zone formed at the titanium surface as a result of its interaction with steel.

As a fracture reflects the structure and properties of the material in a local volume, where the failure occurs, then a kind of fracture can be used as the integral characteristic of condition of the titanium surface layer, as was done during analyzing alpha (gas saturated) layers [1].

To clarify the effect of the diffusion saturation on the structure of surface layers on titanium, the VT6 alloy samples of 20 mm diameter and 3 mm thickness were used, which in contact with samples of steel 20 or 12Kh18N10T were subjected to annealing. Contact surfaces of samples were polished and degreased before annealing. Annealing of the samples was performed within the 850 – 975 °C temperature range at

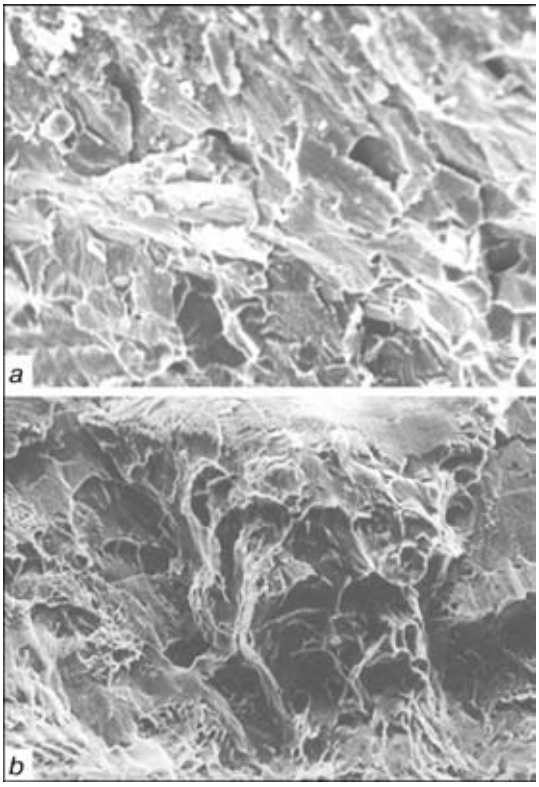

Figure 1. Topography of fracture surface by bending of samples of alloy VT6 in initial state (*a*) and after contact interaction with steel 12Kh18N10T (*b*) (×5000) (reduced by 4/5)

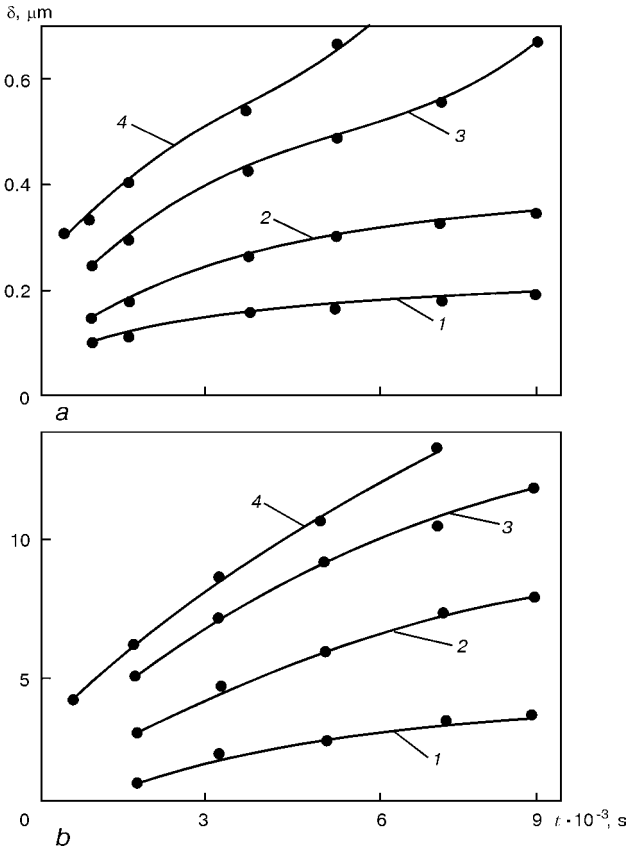

Figure 2. Kinetics of growth of layers on alloy VT6 in the conditions of contact interaction with steels 20 (*a*) and 12Kh18N10T (*b*) at temperature 850 (*1*), 900 (*2*), 950 (*3*) and 975 °C (*4*)

vacuum $8 \cdot 10^{-2}$ Pa and 1 MPa specific compression pressure. After annealing the samples were separated using the device for a shear test, and then they were deformed until failure in the device for a three-point bending to form the fracture surface.

Typical kind of fracture of the VT6 alloy sample in initial state is given in Figure 1, *a*. The fracture surface shows a tough nature of fracture across the entire section of the sample. The fracture surface has tear ridges whose location and direction show that the crack was initiated on contact surface examined and propagated inside the sample.

Two zones are revealed in the structure of fractures of titanium samples after their contact interaction with steel 12Kh18N10T. First of them is brittle, corresponding to the crack propagation in the embrittled part of the diffusion layer (Figure 1, *b*). The second of them is tough, having a typical dimpling structure and corresponding to the crack propagation in titanium in that part of the diffusion layer in which the concentration of interstitial impurity atoms (iron, nickel, chromium and others) was insufficient for its embrittlement.

The embrittled layer in fracture, formed according to a spalling mechanism looks as an integral part of a material-substrate. At its thickness $\delta < 3$ μm the spalling surface looks as a continuous band, and at large sizes of the embrittled zone it consists of a set of facets of a transcrystalline fracture (Figure 1, *b*).

With increase in temperature T and time of annealing, t, the thickness of the embrittled layer $\delta = f(t)$ is increased monotonically to a definite size. The data, obtained by a direct measuring of the embrittled layer from the fractograms of fractures, are given in Figure 2, *a*. In logarithmic coordinates the graphs of relation $\ln \delta = f(\ln t)$ are close to straight lines. This makes it possible to consider that the process of growth of embrittled layers on alloy VT6 during annealing in contact with steel 12Kh18N10T is governed by a parabolic law $\delta^m = K_1 t$, characterized by exponent m and constant K_1. The latter can be considered an exponential function of temperature in accordance with a concept about a diffusion nature of the process

$$K_1 \sim \exp(-E/RT),$$

where E is the energy of activation of the process of an embrittled layer growth; R is the gas constant; T is the temperature, K.

The estimation of effective energy of activation of the process of formation of the embrittled layers using a slope of relation $\ln K_1 = f(1/T)$ (Figure 3, *a*) gives value of order 240 kJ/mole, close to the energy of activation of process of diffusion of iron, nickel and chromium in titanium, which, according to [3], amounts to 215, 235 and 207 kJ/mole, respectively. At atomic content of TiFe up to 5 % it is equal to 165 kJ/mole, and at its increase up to 15 % it reaches 242.8 kJ/ mole [4]. This makes it possible to assume that, during the contact interaction of titanium with steel 12Kh18N10T, the formation of embrittled layers on the surface of VT6 alloy is caused by a diffusion

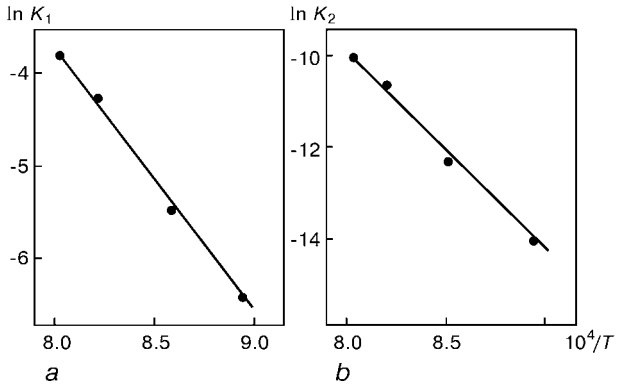

Figure 3. Relationships between the coefficients K_1 and K_2 of the process of growth of embrittled layers on titanium at its contact interaction with steels 12Kh18N10T (*a*) and 20 (*b*) and annealing temperature

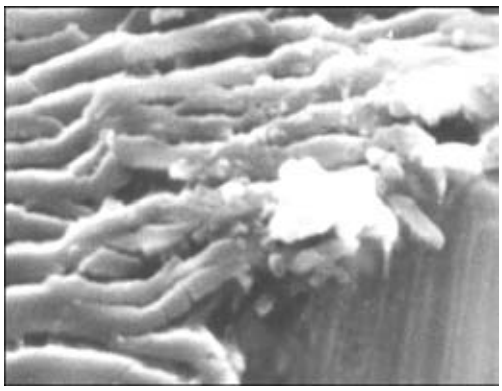

Figure 4. Microstructure of fractures of alloy VT6 after contact interaction with steel 20 (×15000) (reduced by 4/5)

of iron, chromium and nickel into titanium, and a growth of embrittled layers is controlled by the processes proceeding in the diffusion zone which contains compounds of the TiFe type.

To make the quantitative estimation of effect of temperature and annealing duration on the thickness of forming embrittled layers the empiric relationship can be used

$$\delta^2 = [2.8 \cdot 10^8 \exp(-240000/RT)]t, \ \text{мкм}^2.$$

There are thin embrittled layers at the surface of titanium samples after their contact interaction with steel 20, which, due to their lower ductility as compared with the parent metal are cracked during deformation and failure of the samples (Figure 4). However, even at ×15000 magnification it is difficult to measure the thickness of this layer in the fracture due to its small value. Therefore, relation was used for the quantitative estimation [5]

$$\delta = l_{av}/4.2,$$

where l_{av} is the average value of distance between cracks formed in the zone of deformation which is determined from fractograms using 8 – 10 measurements and by averaging the results obtained.

Experimental data on kinetics of growth of embrittled layers, obtained in determination of their thickness by cracking during deformation are given in Figure 2, *b*. At temperatures 900 °C and lower the relations $\delta = f(t)$ have an attenuation nature. The same kind of kinetic curves at higher temperatures (950 – 975 °C) is preserved for the embrittled layers of $\delta \le 0.5$ μm. At further increase in thickness of the embrittled layers the curves are deviated to the side of rising (see curves *3* and *4* in Figure 2, *b*), that makes it possible to state the change of process which controls the growth of the embrittled layers on the alloy VT6.

When plotting a graph of relation $\delta = f(t)$ in logarithmic coordinates, on the basis of experimental data, all the points at $\delta \le 0.5$ μm are well imposed on the straight lines. In addition, the contangent of the angle of inclination of the latter is close to 3, i.e. process of formation of the embrittled layers on alloy VT6 at a contact interaction with steel 20 can be described by a parabolic relation $\delta^m = K_2 t$, where $m = 3$, and K_2 is the constant of growth of the embrittled layers. Graph of relation $\ln K_2 = f(1/T)$ represents a straight line (Figure 3, *b*), whose slope shows that effective energy of activation of the process of growth of the embrittled layers on alloy VT6 at its contact interaction with steel 20 is 348 kJ/mole.

Results of X-ray analysis showed that during titanium interaction with steel 20 a titanium carbide is formed in the zone of contact [2]. According to data, given in [6], the energy of activation of carbon diffusion in titanium is 138, while in titanium carbide it is 347 kJ/mole that is close to our value. Therefore, it is possible to assume that the growth of the embrittled layer under the experimental conditions was controlled by the diffusion of carbon in a carbide-containing layer whose presence is interlocking or, at least, makes the diffusion of iron into titanium difficult. Evidently, this can explain so large difference (by three orders) in constants of growth of embrittled layers on titanium at its contact interaction with steels 20 and 12Kh18N10T.

The observed deviation in run of kinetic curves $\delta = f(t)$ (see Figure 2, *b*) from relation $\delta^3 = K_2 t$ at increase in time of interaction t of titanium with steel 20 ($t > 90$ min at 950 °C and $t > 60$ min at 975 °C) should be associated with the development of diffusion processes in a surface layer of titanium. At a limited content of carbon in the contact zone, determined by chemical composition of steel 20, the increase in temperature and time of annealing leads to the decrease in carbon concentration in the diffusion layer due to its dissolution in the metallic base of titanium and decrease in interlocking (with respect to iron) properties of the embrittled layers. This is accompanied by the development of the process of diffusion of iron into titanium and more intensive growth of the embrittled layers. Thus, the growth of the embrittled layers in these conditions will be controlled here by the diffusion of iron in titanium, but not a carbon in the carbide-containing layer.

To make the quantitative estimation of effect of temperature and duration of annealing on the thickness of formed embrittled layers (at $\delta < 0.5$ μm) on

alloy VT6 at its contact interaction with steel 20 the following relationship can be used:

$$\delta^3 = [1.5 \cdot 10^{10} \exp(-348000/RT)]t.$$

CONCLUSIONS

1. It was established by the method of a scanning microscopy that the embrittled diffusion layers are formed on the titanium surface during the process of a contact interaction of alloy VT6 with steels. Thickness and structure of these layers depend on the chemical composition of steel and temperature-time conditions of treatment.

2. In contact of alloy VT6 with steel 12Kh18N10T the process of formation of the embrittled layers on the titanium alloy is controlled by a heterodiffusion of components of this steel and titanium in the diffusion zone containing intermetallics, while in contact with steel 20 it is controlled by a diffusion of carbon in a carbide-containing layer, interlocking the iron diffusion into titanium.

3. At a limited carbon content in the zone of contact, determined by the chemical composition of steel 20, the increase in temperature ($T \geq 950$ °C) and time of contact interaction ($t > 60$ min) leads to the weakening of interlocking properties of embrittled layers as to the iron. The growth of the embrittled layers under these conditions will be controlled by the diffusion and solubility of iron in titanium.

REFERENCES

1. Bondar, A.V., Peshkov, V.V., Kireev, L.S. *et al.* (1998) *Diffusion bonding of titanium and its alloys*. Voronezh: VSU.
2. Fedorov, S.N., Bondar, A.V., Peshkov, V.V. *et al.* (2000) Contact of titanium components with steel fixture in diffusion bonding. *Avtomaticheskaya Svarka*, **1**, 23 – 26.
3. Charukhina, K.E., Golovanenko, S.A., Masterov, V.A. *et al.* (1970) *Bimetal joints*. Moscow: Metallurgia.
4. Tsvikker, U. (1979) *Titanium and its alloys*. Moscow: Metallurgia.
5. Peshkov, V.V., Del, G.D., Orlova, L.M. *et al.* (1986) Determination of depth of oxidized layer embrittled part at the titanium surface. *Zavod. Laboratoria*, **9**, 75 – 77.
6. Vulf, B.K. (1969) *Heat treatment of titanium alloys*. Moscow: Metallurgia.

METHOD FOR ESTIMATION OF ACCELERATION PARAMETERS OF PLATES IN A MULTILAYER STACK DURING EXPLOSION WELDING

S.V. KUZMIN, V.I. LYSAK and **I.A. SALOMATIN**
Volgograd State Technical University, Volgograd, Russia

ABSTRACT

The new calculation-experimental method has been developed for estimation of collision velocity at the initial stage of acceleration for the second and next interfaces in multilayer metal composite materials during explosion welding. It is shown that to calculate collision velocities at the second and next interfaces it is necessary to make allowance for an increase in momentum of the system caused by external forces affecting it within a short period of time between collision at the previous interface and «going out» of the stack welded to a gently sloping acceleration region.

Key words: *explosion welding, acceleration of plates, high-velocity collisions, composite materials, investigations*

The so-called simultaneous method is indicated for a number of reasons for explosion welding of multilayer composite materials. With this method part of the energy released in explosion of one captive explosion charge is spent for plastic deformation of metal at all interfaces in the stack being welded [1], which leads to formation of a physical contact and activation of the mating boundaries in a metal joint. This requires precise portioning of energy input to each interface in a composite material welded, which is needed to provide identical strength of the joints between the layers, on the one hand, and minimize structural and chemical heterogeneity, on the other hand. This portioning provided by varying the layer-by-layer collision velocities V_{c_i} presents a problem, which is solved, as a rule, in a very rough approximation using calculation models (neglecting the shock-wave processes occurring in a system of colliding elements) [2 – 6]. According to these models, during explosion welding after the i-th event of collision the stack consisting of $i + 1$ plates will immediately acquire some final flight velocity, which is calculated on the basis of the law of conservation of momentum for an isolated system [7]. Therefore, the collision velocity at the second interface of a composite material and those that follow does not depend upon the setting gap between them.

At the same time, it was incontrovertibly proved on the basis of results of experiments conducted using the rheostat method [8] in order to investigate dynamics of the process of acceleration of the explosion welded stack consisting of two model plates [9] that the stack acquired some acceleration velocity, depending upon the initial conditions, not immediately but within a certain period of time. In this connection, the authors of [9] suggested and substantiated the kinematic model of the process of explosion welding of multilayer composite materials. According to this model, acceleration of the stack of metal plates welded in flight occurs in two stages: intensive acceleration within a rather short period of time up to a certain value of velocity, which is calculated, e.g. from the law of conservation of momentum (initial stage), and gradual acceleration of the stack due to residual pressure of the explosive detonation products up to a velocity which is determined by the explosive charge parameters, acceleration phase and setting gap at the composite material interface under investigation. Neglecting the initial stage of acceleration in investigation of the process leads to substantial errors in estimation of the collision parameters at interfaces between layers in a composite material being welded and, hence, involves a problem in realization of optimal properties of multilayer composite materials.

The purpose of this work consisted in development of the calculation-experimental method which would allow estimation of collision velocity at the initial stage of acceleration at the second and next interfaces in multilayer composite materials during explosion welding by avoiding the use of special measurement instruments.

The method developed is based on the following prerequisites. Numerous experimental data show that sizes of the waves generated within the joining zone during explosion welding greatly depend upon the high-velocity collision parameters [10, 12 – 14] and, other conditions being equal, are unambiguously determined by dynamic angle α or collision velocity V_c. On the other hand, parameters of collision of two metal plates can be calculated with an accuracy sufficient for practical application either by using equations of physics of explosion [11] derived for the case of unidimensional acceleration of flat elements by the condensed explosive detonation products, or by using dependencies given in [3, 8] for the case of two-dimensional acceleration. Then the velocity of collision of the elements welded at the investigated interface between layers of a composite materials (starting from the second interface) can be estimated by comparing

Initial experimental parameters

Interface investigated	*Q-ty of interfaces in composite material*	*Layer thickness, mm*	*Gaps at interface, mm*	*Collision velocity, m/s*
1st	1	3.6 + 3.6	0.1 – 1.0	275 – 650
2nd	2	1.8 + 1.8 + 3.6	0.1 – 1.0 (h_1 = 2 mm)	V_{c_1} = 1060

Notes: 1. Layer material — aluminium ADO. 2. Detonation velocity D = 3420 m/s. 3. Explosive charge height (ammonite No.6ZhV) is 30 mm.

parameters of the waves formed at this interface (e.g. wave lengths λ) with the corresponding parameters of the zone of joining of the two-layer billets welded by ensuring stable mass characteristics of the plates, height of the charge, detonation and contact point velocity, kept constant from series to series.

Consider the suggested method for determination of the collision velocity of the plates at the second interlayer between layers of a three-layer composite material in explosion welding, the algorithm of performing of which is shown in Figure 1 (in the case of welding composite materials with more layers the sequence of determination of V_{c_i} will be the same).

At the first stage, the dependence of lengths λ of the waves generated in explosion welding of two-layer billets upon the collision velocity V_c varied in the series of the experiments under consideration over a range of 275 – 650 m/s by discretely varying the setting gap h from 0.1 to 1.0 mm (Table) was experimentally determined for the preliminarily selected materials and their thickness. Then the dependence of the wave length upon the collision velocity, λ = = f(V_c) (Figure 1, *c*), was plotted for specific experimental conditions by comparing calculation data of the collision velocities V_c, which are also the function of the setting gap [5], V_c = f(h) (Figure 1, *a*) with

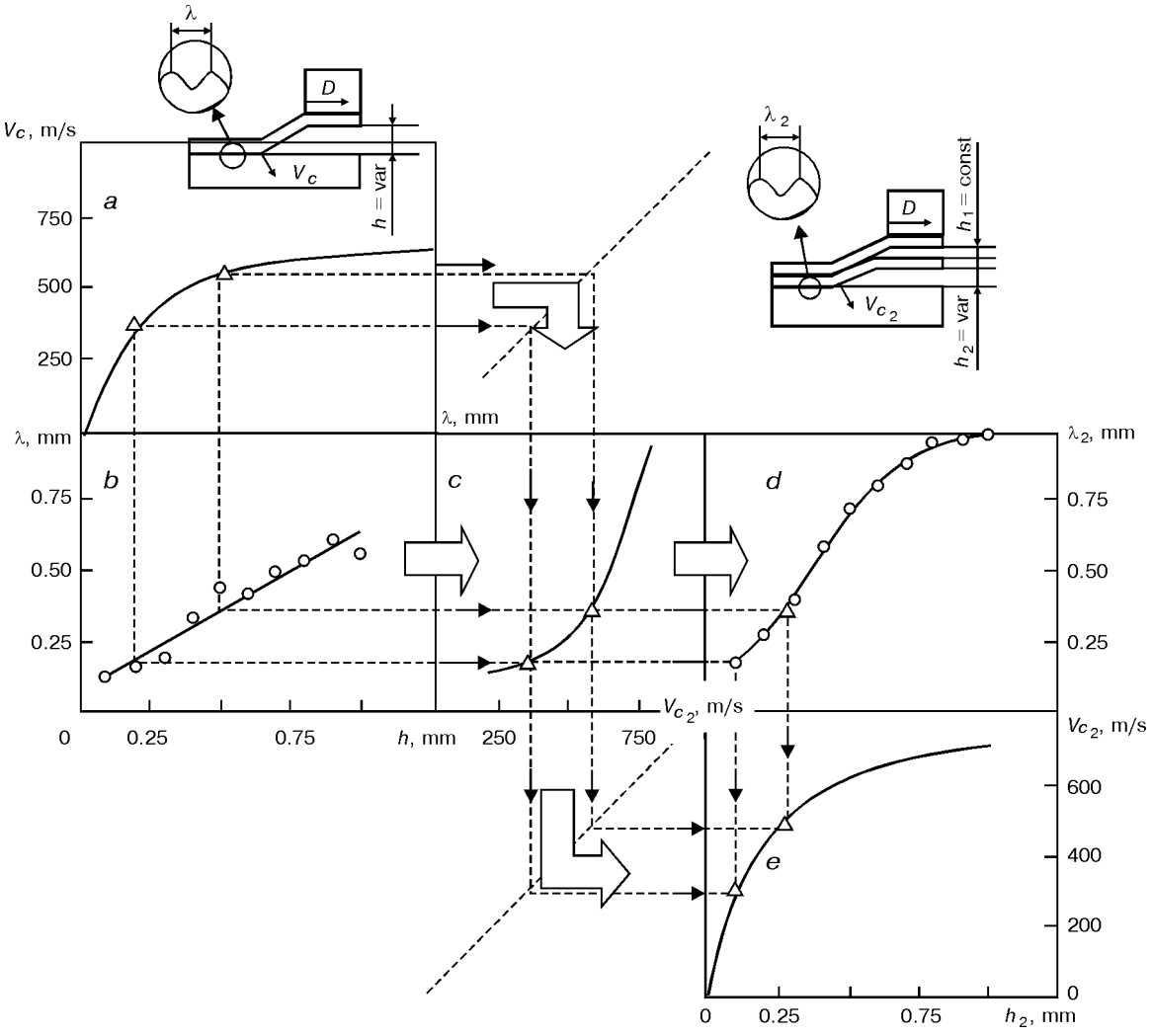

Figure. 1. Algorithm of the method for calculation-experimental plotting of the curve of acceleration V_{c_2} = f(h_2) for the second interlayer in explosion welding of a three-layer composite material (*a* – *e* — see descriptions in the text)

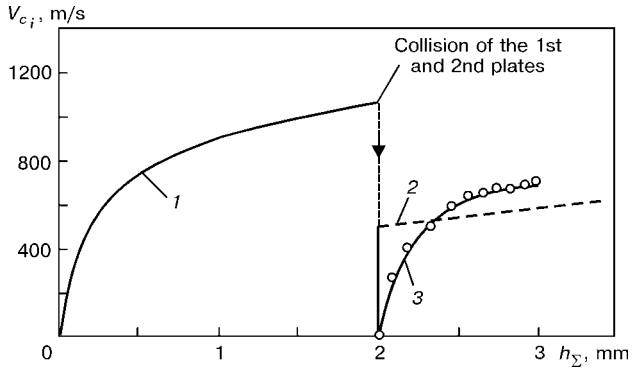

Figure 2. Kinetics of acceleration of elements of the three-layer stack of aluminium plates: *1* — curve of acceleration of the flyer plate (δ_1 = 1.8 mm) [10]; *2* — curve of acceleration of the stack of the two plates welded ($\delta_1 + \delta_2$ = 1.8 + 1.8 mm) [15]; *3* — initial region of acceleration of the stack of the two plates welded ($\delta_1 + \delta_2$ = 1.8 + 1.8 mm) (experimental data)

experimental results relating the wave length with the setting gap, $\lambda = f(h)$ (Figure 1, *b*).

The next stage included explosion welding of a three-layer stack of plates of the same material at a certain constant setting gap in the composite material, h_1, at the first interface (in our experiments it was 2 mm) and at a discretely varied gap h_2 at the second interface, equal to 0.1 – 1.0 mm (see the Table). In this case the obligatory experimental condition was that the total thickness of the first and second plates in the three-layer stack had to be equal to thickness of the flyer plate used at the first stage of the series of the said experiments.

The graphical dependence $\lambda_2 = f(h_2)$ (Figure 1, *d*) was plotted from wave lengths λ_2 obtained for different values of h_2 at the second interface, while the combined solution of the latter using curve $\lambda = f(V_c)$ (Figure 1, *c*) was employed for plotting the curve showing the relationship between the collision velocity at the second interface and initial gaps at it, $V_{c_2} = f(h_2)$ (Figure 1, *e*).

Then the comprehensive picture of layer-by-layer variations in the collision velocities of elements welded in the three-layer stack as a function of the total gap h_Σ (Figure 2), which is a particular kinematic model of explosion welding [9] of the composite material investigated for a given setting gap at its first interface (in our case h_1 = 2 mm), was obtained by combining the acceleration curves $V_{c_1} = f(h_1)$ and $V_{c_2} = f(h_2)$.

Analysis of the Figure shows a substantial difference between the calculated and experimental acceleration curves for the second interface (Figure 2, curves *2* and *3*). At a small gap h_2, which is not in excess of 0.3 – 0.4 mm, the calculated values of $V_{c_2}^{cal}$ (curve *2*) are substantially overrated, as compared with the experimental values of $V_{c_2}^{exp}$ (curve *3*). Besides, the lower the values of h_2, the larger the differences. This fact following the natural laws was noted earlier [9]. Therefore, it should be taken into account in specifying conditions for explosion welding of multilayer composite materials, i.e. limiting the minimum permissible gaps at the second and next interfaces of the composite material, thus avoiding the substantially underrated realistic collision velocities, as compared with the calculated ones.

If the gaps at the second interface are larger than 0.4 – 0.5 mm, the picture observed is different. Part of the experimental acceleration curve is located above the calculated one, being more than 100 m/s higher at h_2 = 1 mm, despite the fact that the latter is plotted with allowance for the effect of residual pressure of the explosive detonation products after collision of the first two plates and for the part of the charge energy which was actually consumed until this moment of time [6, 15]. The detailed analysis of the calculation methods for determination of collision velocities at the second and next interfaces of the explosion welded composite material [6, 15] made it possible to reveal in them one important drawback. It is associated with a prerequisite of a sudden change in the velocity of flight of the stack of plates welded after each collision event until achieving the values calculated from the law of conservation of momentum for an isolated or closed system. This law is valid only for the case where the system of the plates colliding during explosion welding is not affected by any external force or where the effect of such a force is compensated for [16] and is a particular case of the law of conservation of momentum. Whereas in the real case the system of colliding bodies is constantly «topped up» by a sort of a pulse of the force which is external relative to it, and which is determined by the pressure of the detonation products acting on the surface of the flyer plate and its duration. Allowing for this circumstance, the calculated velocity of the stack consisting of two plates welded in flight can be represented as follows:

$$V_2 = \frac{\rho_1\delta_1 V_{c_1} + \int\limits_{\tau_1}^{\tau_2} p(\tau)d\tau}{\rho_1\delta_1 + \rho_2\delta_2}, \qquad (1)$$

where ρ_1 is the density of the flyer plate; δ_1 is the thickness of the flyer plate; $\rho_1\delta_1$ and $\rho_2\delta_2$ are the unit masses of the flyer and intermediate plates, respectively, in the three-layer stack and $\int\limits_{\tau_1}^{\tau_2} p(\tau)d\tau$ is the specific (related to a unit surface area of the flyer plate) pulse of the external force per time interval $\tau_1 - \tau_2$ characterizing an increment in momentum of the system.

Evaluate now an increment in momentum, which is neglected by the existing calculation methods, of the system of two plates welded in flight during the τ_1 time passed from the moment of collision of the first two plates until the moment of acceleration τ_2, of the stack to a velocity calculated from the law of conservation of momentum (Figure 3). For any section of the welded stack considered the τ_1 time that

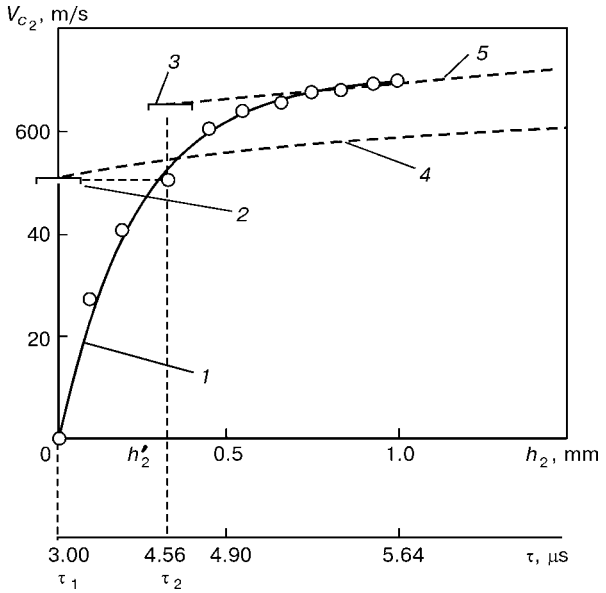

Figure 3. Kinetics of acceleration of the two-layer stack of aluminium plates at the second interface: *1* — experimental acceleration curve; *2, 3* — initial velocity of the two-layer stack, V_2, calculated from the law of conservation of momentum with and without allowance for its increment for a time period of $\tau_1 - \tau_2$, respectively; *4, 5* — acceleration curves with and without an increment in momentum of the system of the interacting plates according to [15], respectively

passed from the moment of exit of the detonation wave from the explosive charge and its entrance into this section to the moment of beginning of movement of the rear surface of the second (intermediate) plate consists of the time of acceleration of the flyer plate to its collision with the second plate, τ_1', and the time of beginning of movement of the rear surface of the second plate, τ_1'', and can be rather precisely determined from the equations of physics of explosion [10]

$$\tau_1 = \tau_1' + \tau_1'' = \frac{h_1}{\eta_1 D}\left[1 + \eta_1 + \sqrt{1 + 2\eta_1\left(1 + \frac{H}{h_1}\right)}\right] + \frac{\delta_2}{c_{0_2}}, \quad (2)$$

$$\eta_1 = \frac{16}{27}\frac{\rho_{ex} H}{\rho_1 \delta_1}, \quad (3)$$

where h_1 is the setting gap at the first interface of the composite material welded; D is the detonation velocity; H is the explosive charge height; ρ_{ex} is the explosive density and c_{0_2} is the velocity of sound in the second plate.

The τ_2 time can be calculated by integration of part of the experimental curve of acceleration of the two-layer stack, $V_{c_2}^{exp} = f(h_2)$ (Figure 3, curve *1*) by h in a region from 0 to h_1' (Figure 3):

$$-\tau_2 = \tau_1 + \int_0^{h_2'} V_{c_2}^{exp}(h)dh. \quad (4)$$

For specific experimental conditions (see the Table) the calculated values of τ_1 and τ_2 were 2.7 + + 0.3 = 3.0 and 3.00 + 1.56 = 4.56 μs, respectively.

Now calculate the unknown pressure pulse acting on the surface of the flyer plate during a time of 3.00 – 4.56 μs. For this we will use the calculated

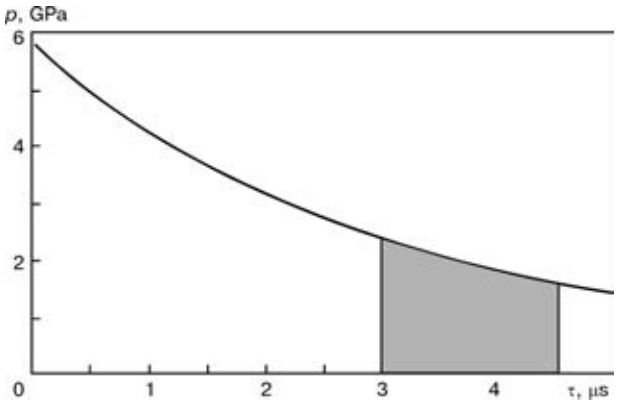

Figure 4. Decrease in pressure acting on the surface of the flyer plate with time according to [10]

dependencies from [10] and plot the curve $p = f(t)$ characterizing the fall of pressure with time (Figure 4). In this case the count of time begins from the moment of exit of the detonation wave and its movement to the surface of the flyer plate, i.e. $\tau = H/D$ (Figure 3, curve *2*)

$$p = \frac{64}{27} p_i \left(\frac{H}{D\tau}\right)^3, \quad (5)$$

$$p_i = \frac{1}{4}\rho_0 D^2, \quad (6)$$

where p_i is the detonation wave pressure and ρ_0 is the initial density of the explosive.

By numerical integration of the dashed region (Figure 4) delineated by curve $p = f(\tau)$, the axis of abscissas and times of 3.00 and 4.56 μs found earlier, determine the value of the specific pulse of the external force

$$\int_{\tau_1}^{\tau_2} p(\tau)d\tau,$$

acting on the system of the colliding plates during an indicated time period. In our case the specific pulse is equal to about 2800 kg/(m·s), which yields an increment of about 140 m/s in the calculated collision velocity. The latter is in satisfactory agreement with the experimental data (see Figure 3).

CONCLUSIONS

1. The developed calculation-experimental method based on comparing sizes of waves generated at a given interface with the corresponding parameters of the zone of joining of the two-layer billets allows estimation of the collision velocity at the initial stage of acceleration for the second and next interfaces of the multilayer metal composite materials during explosion welding.

2. It is shown that to calculate collision velocities at the second and next interfaces of a composite material, it is necessary to allow for an increment in momentum of the system caused by forces acting on it during a short period of time between collision at

the previous interface and exit of the stack welded to a quiet regions of acceleration.

REFERENCES

1. Lysak, V.I., Kuzmin, S.V. (1998) Basic methods and parameters of explosion welding of laminated composite materials (LCM). In: *Int.-Inst. Transact. of Volgograd State Technical University on Explosion Welding and Properties of Welded Joints*. Volgograd: VSTU.
2. Belyaev, V.I., Kovalevsky, V.N., Smirnov, G.V. *et al*. (1976) *High-rate deformation of metals*. Minsk: Nauka i Tekhnika.
3. Deribas, A.A. (1972) *Physics of strengthening and explosion welding*. Novosibirsk: Nauka.
4. Sonnov, A.P., Trykov, Yu.P. (1973) On calculation of parameters of explosion welding of multilayer joints. *Fizika i Khimiya Obrab. Materialov*, **4**, 128 – 133.
5. (1984) *Shock waves and phenomena of high-rate deformation of metals*. Ed. by M.A. Meyers, L.E. Murr. Moscow: Metallurgia.
6. Shmorgun, V.G., Sonnov, A.P., Trykov, Yu.P. *et al*. (1997) Evaluation of collision parameters in explosion welding of multilayer composite materials. In: *Int.-Inst. Transact. of Volgograd State Technical University on Explosion Welding and Properties of Welded Joints*. Volgograd: VSTU.
7. Aleksandrov, E.V., Sokolinsky, V.B. (1969) *Applied theory and calculations of shock systems*. Moscow: Nauka.
8. Kuzmin, G.N., Mali, V.I., Paj, V.V. (1972) On acceleration of flat plates with layers of condensed explosives. *Fizika Goreniya i Vzryva*, **4**, 558 – 562.
9. Kuzmin, S.V., Lysak, V.I., Starikov, D.V. (1994) Kinetics of collision of metal plates in a multilayer stack during explosion welding. *Prikladnaya Mekhanika i Tekhn. Fizika*, **5**, 173 – 175.
10. (1975) *Physics of explosion*. Ed. by K.P. Stanyukovich. Moscow: Nauka.
11. Kudinov, V.M., Koroteev, A.Ya. (1978) *Explosion welding in metallurgy*. Moscow: Metallurgia.
12. Gordopolov, Yu.A., Dremin, A.N., Mikhajlov, A.N. (1976) Experimental evaluation of dependence of the wave length upon the collision angle during explosion welding of metal. *Fizika Goreniya i Vzryva*, **4**, 601 – 605.
13. Gordopolov, Yu.A., Dremin, A.N., Mikhajlov, A.N. (1977) On the problem of wave generation in high-velocity collision of metal bodies. *Ibid*., **4**, 288 – 290.
14. Lysak, V.I., Kuzmin, S.V. (1991) Basic principles of transition to wave-free conditions of formation of joints in explosion welding. In: *Int.-Inst. Transact. of Volgograd State Technical University on Explosion Welding and Properties of Welded Joints*. Volgograd: VSTU.
15. Kuzmin, S.V., Lysak, V.I., Salomatin, I.A. *et al*. (1998) Method for calculation of collision velocities in explosion welding of multilayer composite materials. In: *Proc. of Conf. of Volgograd State Technical University on Laminated Composite Materials*. Volgograd: VSTU.
16. (1983) *Physical encyclopedia*. Ed. by A.M. Prokhorov. Moscow: Sov. Ents.

ACOUSTIC EMISSION OF THE WELDING ARC (REVIEW)

Yu.N. LANKIN
The E.O. Paton Electric Welding Institute, NASU, Kyiv, Ukraine

ABSTRACT

Issues concerning generation of acoustic emission in welding, its relationship with the welding process parameters and quality are considered. Possibilities of using acoustic emission for monitoring and automatic adjustment of the welding process are shown.

Key words: *acoustic emission of the arc, monitoring, diagnostics, control*

Dependence of signals of acoustic emission of the arc (AEA) upon voltage, current, arc length and anode material was demonstrated as far back as 1944 [1]. Initially, the noise of the arc was investigated in terms of its harmful effect on the welder's organism. The total level of sound pressure and spectral composition of acoustic emission of the arc were determined in welding and cutting [2 – 9]. Since the end of the 1970s the work has been conducted on investigation of acoustic emission of the arc for monitoring and diagnostics of the welding processes [10 – 16]. In the last decade the papers have been published on investigation of the AEA signals for automatic adjustment of the welding process [17 – 27]. Investigated were CO_2 welding [10, 11, 13, 28], MIG [10, 11, 15, 18, 19], TIG [10, 12, 14, 17], percussion capacitor-discharge arc welding [16] and oxygen and acetylene cutting [15].

Physical aspects of generation of AEA in welding. The sources of sound in arc welding are the arc column, weld pool, welding device mechanisms and shielding gas. The arc noise constitutes the major part of AEA.

Temperature and, therefore, density of gas in the arc column differ by a few orders of magnitude from those occurring in ambient air. Therefore, from the standpoint of acoustics, the arc is an object with rigid walls, the pulsations of which lead to generation of sound waves.

The cause of variations in sizes of the arc column is oscillation of the current or, to be more precise, power of the arc. In turn, the arc current oscillates because of its programmed variations, pulsations of voltage of the power source, and variations in the arc length in formation of droplets, arc extinction and ignition during welding with short circuiting of the arc gap.

Relationship between the arc column size and current is shown experimentally in [14]. Investigations were conducted with the arc burning in argon by varying the current in accordance with a program following the certain laws. Geometrical sizes of the arc were determined by high-speed filming. The arc current was registered in an oscillogram which was made in synchronism with the latter. Figure 1 shows variations in a relative cross section area of the arc, S/S_{max}, with time at modulation frequency f_p, amplitude value of the current I_p = 150 A and base current of 50 A. They exactly repeat the shape of the current for all types of its modulation.

In turn, variations in the arc surface with current (power) cause AEA. Figure 2 [12] shows records of typical sound waves generated by the arc at different shapes of pulsations of the current. It is seen that the sound pressure is proportional to the rate of variations in the arc current or, to be more precise, to the radial rate of oscillations of the lateral surface of the arc column.

In short-arc CO_2 welding the main sound waves emerge at the moment of excitation of the arc [10] after short circuiting of the arc gap (Figure 3). Break of bridge of molten metal at the end of short circuiting is of an explosive character and accompanied by a shock wave propagating at a velocity which is somewhat higher than the velocity of sound. In this case the shape of the generated sound signal greatly depends upon the transmission band of a microphone [29].

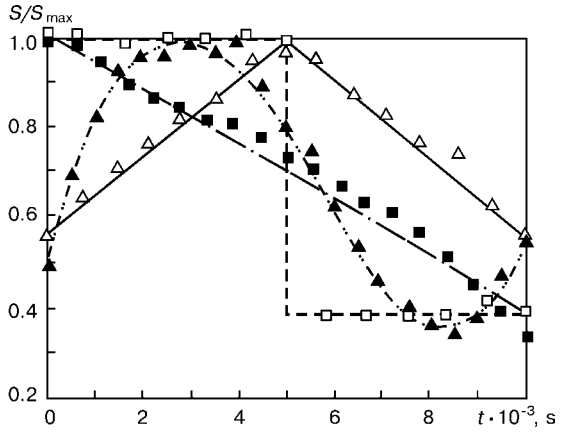

Figure 1. Dependence of the relative cross section area of the arc in TIG welding upon the time at different shapes of pulses of the current: ❐ – rectangular; ■ – serrated; Δ – triangular; ▲ – sinusoidal

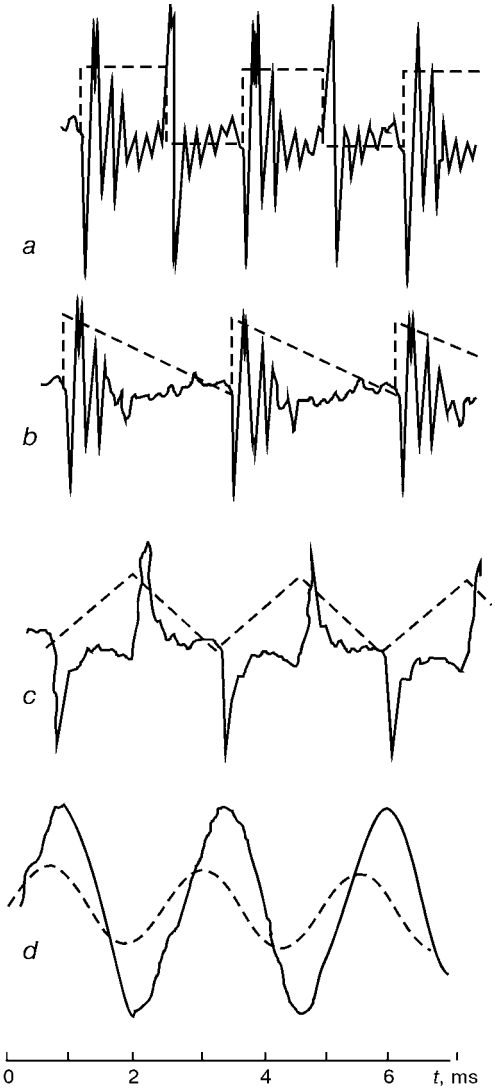

Figure 2. Typical sound waves at different shapes of modulation of the current (f_p = 500 Hz, I_p = 100 A): *a* — rectangular; *b* — serrated; *c* — triangular; *d* — sinusoidal

In TIG welding at an alternating current of both rectangular and sinusoidal shape the shock waves are identical to those shown in Figure 3. They are excited at the current passing through a zero value, i.e. at

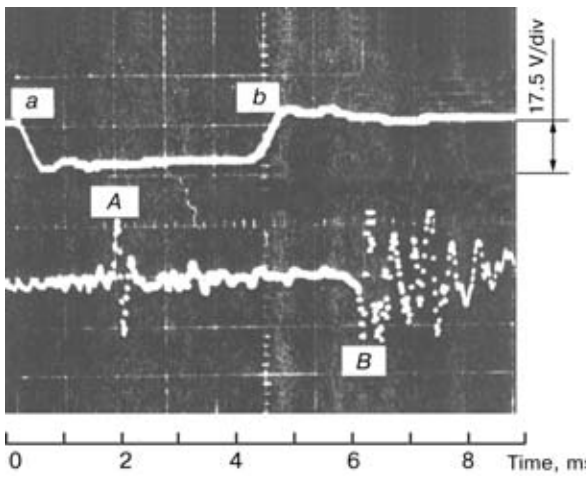

Figure 3. Typical oscillograms of arc voltage (*upper curve*) and arc sound intensity (*lower curve*) in short circuiting during CO_2 welding: *a*, *A* — short circuiting; *b*, *B* — break of the bridge

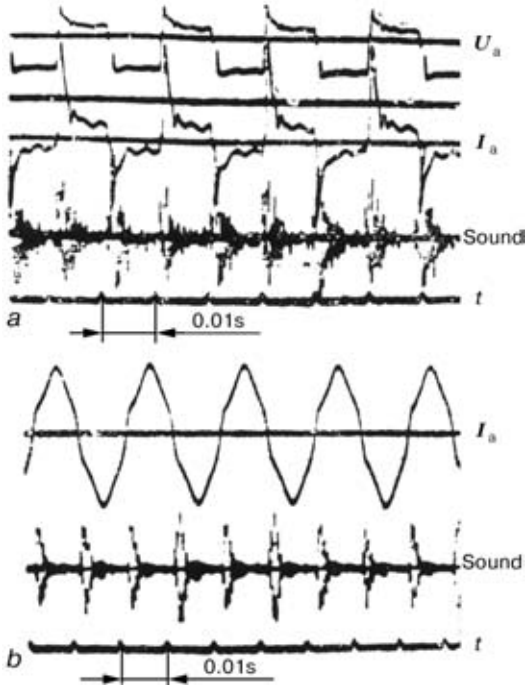

Figure 4. Registration of signals of sound waves in AC TIG welding: *a* — rectangular shape of arc voltage; *b* — sinusoidal current

extinction and repeated excitation of the arc in the case of a change in polarity and at the moment of the most dramatic variation in the current, as shown in Figure 4 [17].

Theoretical aspects of generation of sound waves in welding. It is assumed that in the first approximation the volume of the arc column is proportional to the arc power: $W_a = K_1(I_a U_a)$.

Because of thermal inertia, the arc is an aperiodical link of the first order at a time constant of $T_a = 10^{-4} - 10^{-3}$ s [30 – 32].

Judging from the photos given in [14], a typical size of the arc is 2 – 4 mm. In investigations of AEA the microphone is usually placed at a distance of 40 – 50 cm from the arc, which corresponds to a distance to the welder's ears in the case of manual and semiautomatic welding [4, 9]. At this distance the arc sounds almost as a small spherical source [14]. For such a source the wave equation in the spherical coordinate system has the following form [33]:

$$\frac{\partial^2(r\Phi)}{\partial r^2} = \frac{1}{c}\frac{\partial^2(r\Phi)}{\partial t^2}, \qquad (1)$$

where Φ is the potential of velocity of air particles and c is the sound velocity.

For a spot-type sound source it is solved as follows:

$$\Phi = \frac{1}{r} f(ct - r), \qquad (2)$$

or

$$p = \rho\frac{\Phi}{t} - \frac{\rho c}{r} f', \qquad (3)$$

where f′ is the derivative of function f from argument $(ct - r)$; p is the pressure and ρ is the density of air.

Velocity of the air particles is as follows:

$$v = -\frac{\partial \Phi}{\partial r} = \frac{1}{r}f' + \frac{1}{r^2}f = \frac{p}{\rho c} + \frac{1}{\rho r}\int \rho dt. \qquad (4)$$

In the right part of equation (4) its first term describes the far field and the second term describes the near field. For the far field, which is of interest to us, the sound pressure is proportional to the velocity of the particles.

The shape of the sound wave described by function $p(t)$ is determined from the boundary condition at the surface of a sphere with radius a at $r = a$:

$$\frac{1}{r}\frac{\partial \rho}{\partial r} - \frac{p}{r^2} = \frac{\rho}{4\pi a^2}\frac{\partial \theta}{\partial t},$$

where $\theta = 4\pi a^2 v(t)$ and $v(t)$ are the volume and radial velocities, respectively, at the surface of the sphere.

At non-sinusoidal oscillations of the sphere surface the analytical solution of equation (4) is too cumbersome and hard to interpret. Therefore, the analytical investigation is normally limited to harmonic oscillations of the following type:

$$\theta = \theta_0 e^{-i\omega t}.$$

For the far field

$$p = -i\omega\left(\frac{\rho}{4\pi r}\right)\theta_0 e^{ik(r - ct)},$$

where $k = \omega/c = 2\pi/\lambda$; λ is the wave length and $r >> \lambda$.

The harmonic Fourier analysis allows extension of this solution also to the non-harmonic oscillations.

Therefore, the sound pressure of a small pulsating sphere is determined only by its volume velocity. Shape of the small sound source exerts no effect on the value of the generated sound pressure at large distances. This concerns the welding arc for distances which are of practical interest (more than 0.4 m). As the volume of the arc is proportional to the current (power) of the arc, the sound pressure is proportional to the rate of its variation.

Experimental characteristics of AEA and their relationship with welding parameters. AEA is usually estimated by the level of intensity of the sound, L, dB:

$$L = 20 \lg \frac{p_e}{p_{e0}},$$

where p_e is the effective sound pressure and p_{e0} is the standard level of the effective sound pressure ($2 \cdot 10^{-5}$ Pa/m^2).

Shape of the acoustic waves is normally evaluated from oscillograms of voltage $U(t)$ of a measurement microphone.

Arc power. The effect of the input power of the arc or, to be more precise, U_a at I_a = const, on the level of intensity of the sound is illustrated in Figure 5 [10], where the dashed zone is a boundary of a discrete metal transfer and *D, G* and *S* are the conditions characterized by short circuiting of the arc, drop and spray transfer of the electrode metal, respectively. The dependencies given have the form of a turned *S* letter, which is especially pronounced in MIG welding.

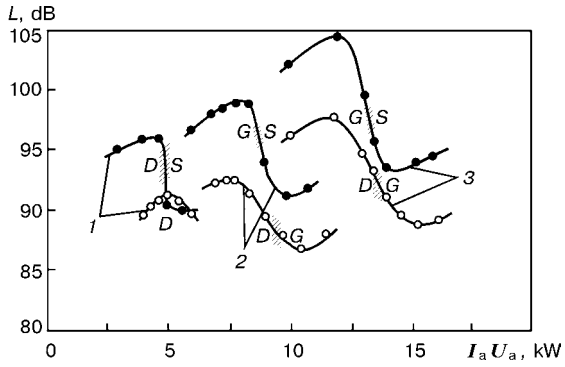

Figure 5. Effect of power of the arc on the level of intensity of the sound in MIG welding (●) and CO_2 welding (○) at I_a = = 200 (*1*), 300 (*2*) and 400 A (*3*); v_w = 20 cm/min

In DC TIG welding AEA does not change within a range of variations in the current from 150 to 250 A at an arc voltage of 19 V. AEA hardly exists in the case of using more perfect (without voltage pulsations) welding power supplies operating at the direct current.

The level of intensity of the sound in TIG welding at a modulated current grows with frequency and amplitude of pulses of the current obeying the following law [12]:

$$p_e \sim I_p^m f_p^n.$$

The values of m and n depend upon the shape of the current pulses: $n = m \approx 0.7$ (for rectangular and serrated oscillations) and $n = m \approx 1.2$ (for triangular and sinusoidal oscillations).

Other conditions being equal, the level of the signal falls with transition from rectangular to serrated, triangular and, finally, sinusoidal oscillations. This should be expected, as it is proportional to the rate of variations in the welding current.

In covered-electrode welding the value of L depends upon the arc length, kind of the welding current and its level, i.e. it increases with an increase in the latter at a constant arc length. The corresponding dependences are shown in Figure 6 [9].

Electrode extension. An increase in the electrode extension [10] in CO_2 welding makes melting of the electrode easier owing to its extra heating by the current flow. However, if the electrode extension is too large, the level of intensity of the sound increases and becomes unstable, and the weld surface becomes uneven. If the value of the electrode extension is kept at an optimal level (normally within a range of 10 – 20 mm), the arc noise becomes stable and low

Welding speed. Dependence of L upon the welding speed is insignificant, and, as it follows from

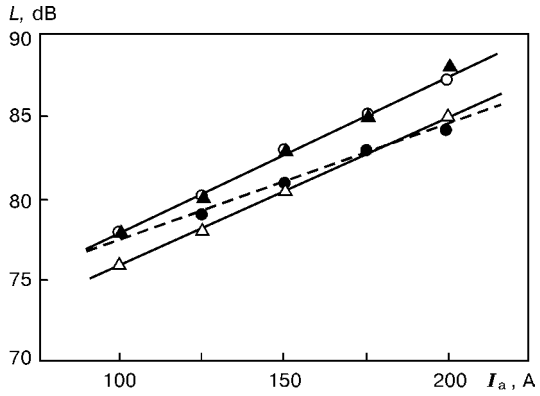

Figure 6. Effect of the current on the level of intensity of the sound in welding using covered electrodes JIS D 4303 4 mm in diameter at the AC and arc length l_a equal to 4 (Δ) and 8 mm (▲), and at the DCSP (●) and DCRP (○) at l_a = 4 mm

Figure 7, it becomes noticeable starting from currents of above 300 A [10]. At a welding speed of 20 cm/min the value of L decreases very rapidly with an increase in U_a. This change in the curves is caused by the fact that at low welding speeds the range of the arc voltages corresponding to a given current is narrower, and, as shown by the high-speed filming, conditions of the drop transfer become more stable owing to a more concave weld pool.

Shielding gas flow rate. The effect of shielding gas flow rate Q within a range of 0 – 25 l/min on L is shown in Figure 8 [10]. At the absence of a shielding gas the level of intensity of the sound becomes constant even in the case of an increasing welding current. In the case of using a gas with its flow rate increased to 15 l/min this characteristic increases until it becomes constant. However, in CO_2 welding at a current of 200 A and voltage of 20 V the value of L slightly decreases.

X-ray analysis of motion patterns of the CO_2 welding process shows that welding conditions are good at a shielding gas flow rate of more than 10 – 15 l/min, i.e. at $L = f(Q)$ going out to a constant level. Therefore, whether the shielding gas flow rate setting is correct or not can be judged from AEA.

Spectral analysis. The sound radiation spectrum, which is a distribution of intensity of the sound by frequency, is important for two reasons. Firstly, the human ear perceives the sound differently at different frequencies. The subjective perception of the sound volume does not coincide with the sound pressure. The volume of the sound falls with an increase in frequency under the same sound pressure and then grows again at frequencies of above 5 kHz. That is why at one and the same integral intensity of the sound the volume and hence the harmful effect on the human organism depend upon the spectral composition of radiation. This is taken into account by GOST 12.1.003–83 «Noise. General safety requirements» and, for example, by the Japanese Standard JCGIH [9].

Secondly, as it has been already noted, an experienced welder can evaluate the welding process by a character of the sound, which is determined to a considerable degree by the spectral composition. Thus, it is suggested that the AEA spectrograms can be used for automatic adjustment and monitoring of welding conditions.

Figure 9 shows typical AEA spectra for different welding and cutting processes. It should be noted that they vary not only with a type of welding and its parameters, but also with time (Figure 9, *h*). Time variations of a spectrum can be avoided by calculation of the effective values on the basis of its realization [34].

To identify a spectrum, it can be represented either by a multicomponent vector [34] or by a set of static parameters, such as maximum and minimum values of peaks, arithmetic mean or root-mean-square value, peak factor, form factor, median, correlation factor, etc. [16].

Other parameters of AEA. In addition to the intensity level and spectrum, many other parameters developed for analysis of random processes [18] are used to characterize AEA:

mean value of amplitudes

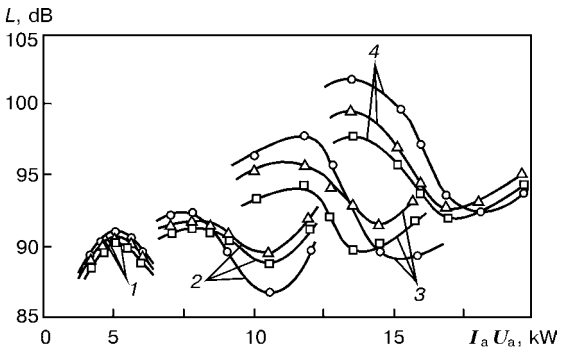

Figure 7. Effect of the input arc power on the level of intensity of the sound in CO_2 welding at a speed of 20 (○), 40 (Δ) and 60 cm/min (❒) and arc current of 200 (*1*), 300 (*2*), 400 (*3*) and 450 A (*4*)

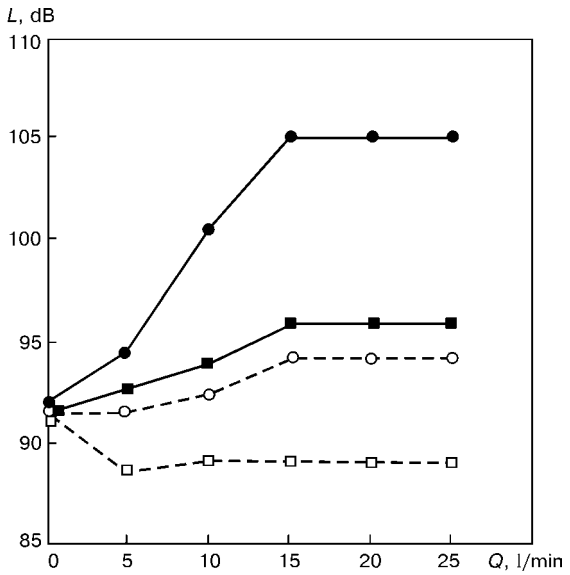

Figure 8. Effect of the gas flow rate on the level of intensity of the sound in MIG welding (●, ■) and CO_2 welding (○, ❒): ●, ○ – I_a = 400 A, U_a = 32 V; ■, ❒ – I_a = 200 A, U_a = 20 V; in all cases v_w = 40 cm/min

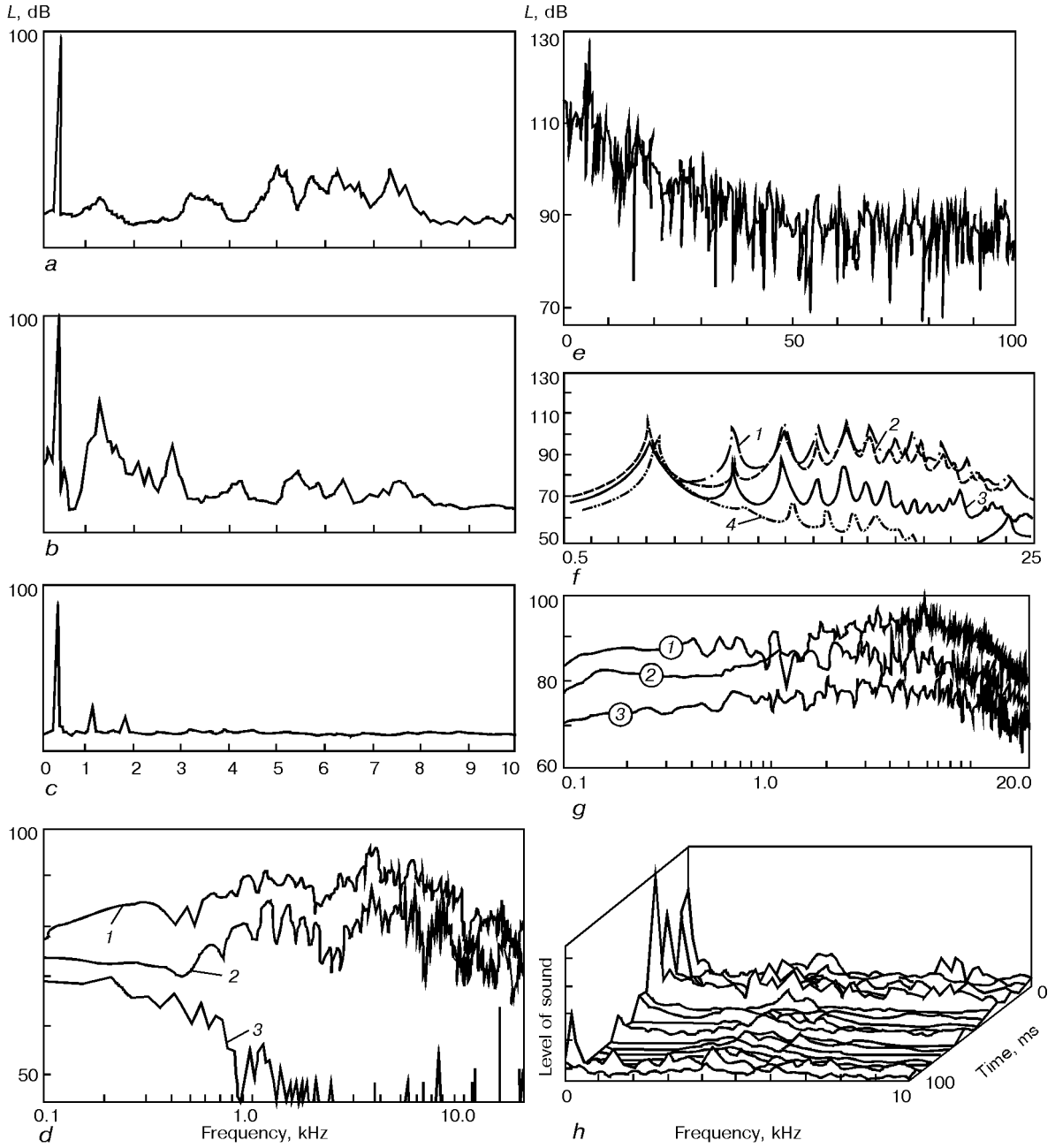

Figure 9. Frequency spectrum of sound signal of the welding arc in different welding methods: CO_2 (*a*); MIG (*b*); TIG (*c*); MAG (*d*) at I_a of ≈ 160 (*1*) and 110 A (*2*) (*3* — background level); percussion arc welding (*e*); modulated-current TIG welding (*f*) (*1* — rectangular; *2* — serrated; *3* — triangular; *4* — sinusoidal); oxygen cutting (*g*) under a pressure of 0.80 (*1*), 0.55 (*2*) and 0.20 MPa (*3*); variation in the frequency spectrum of the arc in SAW with time (*h*)

$$\bar{u} = \frac{1}{N}\sum_{n=0}^{N-1} |u(n)|;$$

square root of amplitudes

$$u_r = \left[\frac{1}{N}\sum_{n=0}^{N-1} \sqrt{|u(n)|}\right]^2;$$

mean-root-square value

$$u_{\text{mrs}} = \left[\frac{1}{N}\sum_{n=0}^{N-1} u^2(n)\right]^{1/2};$$

the highest absolute value

$$\hat{u} = \max |u(n)|;$$

zero intersection frequency

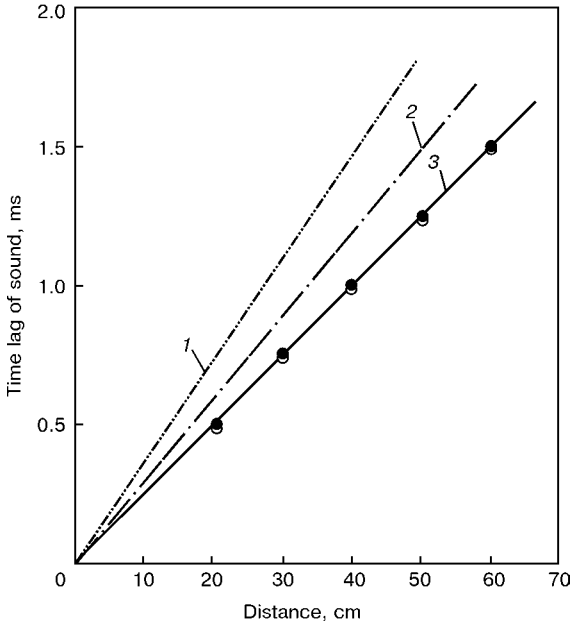

Figure 10. Dependence of the time lag of the sound upon the distance to a microphone in the CO_2 atmosphere (*1*) and in air (*2*) at 15 °C, and the hot arc noise (*3*) in CO_2 welding (● — I_w = = 200 A, U_a = 20 V; ○ — I_w = 300 A, U_a = 24 V)

$$Z = \frac{1}{NT_0} \sum_{n=0}^{N-1} \{\text{sgn}[u(n)] - \text{sgn}[u(n-1)]\},$$

$$\text{sgn}[u(n)] = \begin{cases} 0, & \text{if } u(n) < 0, \\ 1, & \text{if } u(n) \geq 0; \end{cases}$$

form factor $K = u_{\text{mrs}}/\bar{u}$;
peak factor $C = \hat{u}/u_{\text{mrs}}$;
pulse factor $I = \hat{u}/\bar{u}$;
clearance factor $M = \hat{u}/u_r$;
4th root of the Kurtosic parameter

$$\beta^{0.25} = \frac{\left[\frac{1}{N}\sum_{0}^{N-1} u^4(n)\right]^{1/4}}{u_{\text{mrs}}};$$

auto-correlation function [11], etc.

Here $u[n]$ are the discrete samplings of the continuous signal $u(t)$ at $t = nT_0$, where T_0 is the polling period; $n = 0, 1, 2, \ldots, N-1$, N is the realization length.

Using the AEA signals for monitoring and automatic adjustment of the welding process. *Evaluation of the character of electrode metal transfer*. The level of the sound pressure of the arc in MIG and CO_2 welding, as shown in Figure 5, greatly depends upon the arc power. This offers the possibility of more or less reliably evaluating the character of electrode metal transfer for conditions of the immersed-arc, drop or spray transfer. This dependence is most pronounced at low welding speeds. The use of other parameters of AEA holds more promise for this purpose. The investigation results given in [18] show that the reliable identification of the character of metal transfer is provided by zero intersection frequency Z, square root of amplitudes u_r, and form factor K.

The averaged frequency and power spectrum are worthy of the highest attention among the frequency-dependent parameters. In welding with short circuiting of the arc gap the main noise of the arc occurs at low frequency, while in the case of the spray transfer the peaks of power of the sound are observed at frequencies of 7, 11 and 13 kHz.

It should be noted that for practical application of AEA in the automatic adjustment systems, digital processing of its signals should be made much faster [18, 19].

Determination of the arc length and distance from the torch to a workpiece. Described in [22] is a relationship of the AEA parameters with voltage and current of the arc in gas-shielded pulse-arc welding. It is shown that modulation of power leads to modulation of the volume of plasma and, accordingly, to variations in the sound pressure in proportion to the current and voltage derivatives. The level of voltage greatly depends upon the arc length, which made it possible to suggest a regulator which maintains an optimal arc length on the basis of acoustic information.

The sound velocity in the atmosphere is more or less constant. Therefore, microphones fix sound with a small time lag (0.5 – 1.5 ms) after it is generated (see Figure 3). Its duration depends only upon distance l between the microphone and the sound source, i.e. welding arc (Figure 10). The moment of generation of a pulse of the sound pressure can be easily fixed by the signal of the current in gas-shielded pulse-arc welding (see Figure 2) or by the arc voltage in CO_2 welding with short circuiting (see Figure 3). If the microphone is rigidly connected to the welding torch, the time lag between the moments of generation of the microphone signal at a sudden change in the arc current (voltage) is proportional to the distance from the torch to the arc. Frequency of its measurements coincides with frequency of variations in the arc current (voltage) amounting to more than 40 Hz, i.e. the response of the sensor is very fast [35].

Control of stability and optimality of welding conditions by the AEA signals. Investigated in [36] is the MIG welding process using different flux-cored wires. The signal spectra and integral values were digitally recorded. Analysis of average current values allows identification of the drop transfer and immersed-arc conditions, although the spray transfer conditions can hardly be identified. It was noted that the integral values of the AEA signal could be used to control quality of the welding process. However, to realize it directly during the welding process, it is necessary to develop faster and more reliable methods for processing the signals.

Fast Fourier transform was used (not very successfully) to analyse the AEA signals in CO_2 welding [37]. It was revealed that the AEA energy calculated by integrating the sound spectrum by all frequencies

correlates with power of the laser, its focal distance and welding speed.

The use of AEA to control the process in SAW is associated with considerable difficulties. Firstly, visual information is not enough to identify the process quality, as the observations require, e.g. an expensive and often too sophisticated X-ray and infra-red equipment. Secondly, sound emission is screened by a shielding flux. Thirdly, there are interferences caused by a random break of gases through the molten flux. For these reasons control of the metal transfer process in SAW using AEA involves such a refined method as neuron networks [34, 38]. For teaching, the system was shown the AEA spectrograms taken in welding under optimal conditions, as well as spectrograms of weldings performed at voltage, current and speed varied over wide ranges. Optimality of conditions was determined by postweld investigations of samples. The teaching system allowed the use of AEA to identify deviations of the arc voltage [38], current and welding speed from optimal values [39] in real time, i.e. during the welding process.

Some attempts were made earlier to use statistical methods and methods of analysis based on the AEA interpretation rules [23]. However, non-flexibility of these methods under conditions of considerable interferences, along with a limited rate of processing the signals, did not lead to success.

CONCLUSIONS

1. AEA in welding is caused by oscillations of the surface of the arc column, which in turn are caused by oscillations of the arc power.

2. Intensity of the arc noise is proportional to the rate of oscillations of the arc power.

3. All variations in parameters of the welding process influence AEA to an extent to which they influence the rate of oscillations of the arc power.

4. The minimum level of intensity of the sound is found in TIG welding using a power source with a well smoothed current, and the maximum level is found in TIG welding with a modulated rectangular current.

5. Processing the AEA signals makes it possible to obtain in some cases the information on the character of mass transfer of the electrode metal, stability and optimality of welding conditions. Examples of the successful application of AEA in systems for automatic adjustment of the welding process with feedback are unknown.

6. Since AEA is entirely determined by the rate of oscillations of the arc power, it is more convenient to use the arc current and voltage signals for purposes of automatic monitoring and control of the welding process. The methods of statistical analysis and artificial intelligence are equally applicable for processing the electric and acoustic signals.

7. It is likely that the AEA spectra, contrary to the electrical parameters of the arc, contain some extra information on the processes occurring during welding, but so far the investigations conducted fail to prove this.

8. The electrode extension acoustic sensor is a good alternative, although less accurate, to optical sensors.

REFERENCES

1. Schluge, H., Finkelburg, W. (1944) On the hissing of homogeneous carbon arc. *Zeitschrift für Physik*, **122**, 714 – 739.
2. Schlebeck, E., Lopp, Th. (1980) Der Schall als Informationsträger für die Schweißtechnik. *Schweißtechnik*, **6**, 260 – 263.
3. Pfeuffer, A. (1975) Brennschneiden in Hüttenwerken. *Schweißen und Schneiden*, **12**, 496 – 499.
4. Heidemann, W. (1977) Einge Fragen der Gehörschädigung durch Lärm. *Ibid*., **11**, 437 – 440.
5. Press, H. (1976) Messungen des Schallpegels und Massnahmen zum Gehörschutz beim Plasmaschneiden. *Ibid*., **2**, 65 – 68.
6. Eichbauer, H., Schmidt, R. (1982) L
ärm- und Rauchbelastung des Schweißers. *Ibid*., **11**, 535 – 539.
7. Schlebeck, E. (1983) Akustische Verfahrensdiagnose an Preßstumpf- und Schmeltzschweißverfahren. *Schweißtechnik*, **8**, 340 – 343.
8. Erdmann-Jesnitzer, F., Feustel, E., Rehfeld, D. (1967) Akustische Untersuchungen am Schweißlichtbogen. *Schweißen und Schneiden*, **3**, 95 – 100.
9. Futamata, M. *et al*. (1986) *Investigation on welding arc sound. Report 6. Permissible time of arc sound exposure from viewpoint of conservation of hearing acuity*. IIW Doc. VIII-1337–86.
10. Arata, Y., Inoue, K., Futamata, M. *et al*. (1986) *Investigation on welding arc sound. Report 1. Effect of welding method and welding condition on welding arc sound*. IIW Doc. VIII-1340–86.
11. Arata, Y., Inoue, K., Futamata, M. *et al*. (1986) *Investigation on welding arc sound. Report 2. Evaluation of hearing acuity and some characteristics of arc sound*. IIW Doc. VIII-1341–86.
12. Arata, Y., Inoue, K., Futamata, M. *et al*. (1986) *Investigation on welding arc sound. Report 3. Effect of current waveforms on TIG welding arc sound (I)*. IIW Doc. VIII-1342–86.
13. Arata, Y., Inoue, K., Futamata, M. *et al*. (1986) *Investigation on welding arc sound. Report 4. Vibration analysis of base metal during welding*. IIW Doc. VIII-1343–86.
14. Arata, Y., Inoue, K., Futamata, M. *et al*. (1986) *Investigation on welding arc sound. Report 5. Effect of current waveforms on TIG welding arc sound (II)*. IIW Doc. VIII-1344–86.
15. Hahn, O., Rostek, W., Buddle, L. (1985) *Computer-aided analysis of sound emission in the welding and cutting technology*. IIW Doc. 212-625–85.
16. Hahn, O., Rostek, W. (1986) *Computer supported analysis and evaluation of emitted acoustic waves when stud welding with tip ignition*. IIW Doc. 212-664–86.
17. Zhang, J.H., Wang, Q., Cui, H. *et al*. (1985) *Study on arc sound in TIG and plasma welding processes and the possibility of its application in practice*. IIW Doc. 212-610–85.
18. Saini, D., Floyd, S. (1998) An investigation of gas metal arc welding sound signature for on-line quality control. *Welding J*., **4**, 172 – 179.
19. Johnson, J.A., Carlson, N.M., Smartt, H.B. *et al*. (1991) Process control of GMAW: Sensing of metal transfer mode. *Ibid*., 91 – 99.
20. Schlebeck, E. (1983) Acoustic process diagnosis in flash and fusion welding processes. *Schweißtechnik*, **8**, 340 – 343.
21. Manz, A. (1981) Welding arc sounds. *Welding J*., **5**, 23 – 27.
22. Kaskinen, P., Mueller, G. (1986) Acoustic arc length control. Advances in welding science and technology. In: *Proc. of Int. Conf. on Trends in Welding Research*. Gatliburg.
23. Chawla, K.S., Norrich, J. (1992) Real time quality monitoring using analysis of the arc sound. In: *Proc. of 4th Int. Conf. on Computer Technology in Welding*, Cambridge, June. Abington: TWI.
24. Rostek, W. (1990) Investigations on the connection between welding process and airborne noise emission in gas shielded metal arc welding. *Schweißen und Schneiden*, **6**, 96 – 98, 289 – 292.

25. Budde, L. (1991) Analysis and evaluation of sound emission in the welding and cutting technology. *ASME*, **51**, 245 – 250.
26. Inoue, K., Takahashi, Y., Zhang, J. (1993) Measurement of arc sound with burnthrough in MAG welding. *Welding Int.*, **10**, 770 – 775.
27. Futamata, M. (1991) Welding process monitoring by arc sound. In: *Proc. of Techn. Commission on Welding Process of JWS*.
28. Lebedev, A.V. (1991) *Computer-aided control of melting and metal transfer in arc welding.* Dr. Sci. (Eng.) Thesis. Kyiv: PWI.
29. Barborak, D., Richardson, R. (1994) Development of pool dynamics software for weld pool oscillation sensing. In: *Proc. of 5th Int. Conf. on Computer Technology in Welding*, Paris, June.
30. Pentegov, I.V. (1976) Mathematical model of the dynamic electric arc column. *Avtomaticheskaya Svarka*, **6**, 8 – 12.
31. Pentegov, I.V., Sidorets, V.N. (1988) Energy parameters of the mathematical model of the dynamic welding arc. *Ibid.*, **11**, 36 – 40.
32. Pentegov, I.V., Sidorets, V.N. (1992) Evaluation of intensity of sound of the electric welding arc. *Ibid.*, **11/12**, 28 – 31.
33. Skuchik, E. (1976) *Fundamentals of acoustics*. Moscow: Mir.
34. Taylor, K., Stroud, R.R., Harris, T.J. *et al.* (1994) The analysis of airborne acoustics of SAW using neural networks. In: *Proc. of 5th Int. Conf. on Computer Technology in Welding*, Paris, June.
35. Blumschein, E. (1994) Acoustic tuning versus predetermination of parameters for short arc welding. *Ibid.*
36. Chawla, K. (1993) *Objective on line assessment of the performance of flux cored wires by real time computer based monitoring*. Ph. Dr. Thesis, Cranfield Inst. of Technology, U.K.
37. Mao, Y.L. *et al.* (1993) Real time fast Fourier transform analysis of acoustic emission during CO_2 laser welding of materials. *J. Laser Applications*, **2, 3**.
38. McCardle, J.R., Swallow, S.S., Stroud, R.R. *et al.* (1996) The use of arc sound and on line ultrasonic signal processing as a monitoring medium for welding. In: *Proc. of 7th Int. Conf. on Computer Technology in Welding*, Lanaken, Belgium, June.
39. Blumschein, E., Wemer, Ch., Blumschein, J. et al. (1996) A concept for cognitive control of welding processes. *Ibid.*

FERRITIC FILLER METAL FOR WELDING COLD-RESISTANT NICKEL STEELS

K.A. YUSHCHENKO, T.M. STARUSHCHENKO and **V.A. PESTOV**
The E.O. Paton Electric Welding Institute, NASU, Kyiv, Ukraine

ABSTRACT

Given are the results of research and development of wire for welding cold-resistant nickel steels with 6 and 9 % Ni, providing full-strength welded joints with high toughness and ductility values at a temperature of up to 77 K. It is shown that to ensure low-temperature toughness of the weld made using the Sv-OH12VI wire, it is necessary to create conditions for tempering of the weld metal after each pass, which is achieved by making stringer welds by the short- or immersed-arc multipass welding method.

Key words: *multipass welding, tempering, reheating, cold-resistant steels, welding consumables, ductile properties, full strength, deposition coefficient, heat input, residual austenite, low-temperature toughness*

Expansion of the area of application of liquefied gases requires further improvement of equipment for their storage. First of all, this is associated with the necessity to ensure its operational strength and reliability over the entire range of service temperatures. The wide acceptance in the national practice has been gained by steels containing 6 and 9 % Ni. The majority of technological processes of welding such steels provides for the use of high-nickel filler materials (more than 60 % Ni) [1 – 3]. Metal of such welds is characterized by high values of low-temperature toughness and ductility. However, in this case full-strength welded joints are not achieved. The yield strength value at 293 K used to design structural components makes utilization of such steels for the fabrication of cryogenic isothermal tanks inefficient. Some strengthening of the austenitic weld metal can be achieved through alloying it with such elements as nitrogen, molybdenum and tungsten. However, the possibility of strengthening is limited by operational properties of the deposited metal (probability of hot cracking, formation of porosity and other defects).

Improvement of fabrication of cryogenic tanks provides for production of full-strength welded joints in steels containing 6 and 9 % Ni.

Welded joints with strength equal to that of the base metal can be achieved by providing weld metal with phase composition similar to that of the base metal. However, this involves a problem of ensuring low-temperature toughness and ductility of the welds.

In [4] this problem is solved by using welding consumables of the ferritic grade, whose alloying system corresponds to that of the base metal.

The purpose of this work was to develop the commercial technology providing the full-strength welded joints in cold-resistant steels containing 6 and 9 % Ni, by welding using a ferritic filler metal and preserving the high toughness and ductility values over the entire range of service temperatures (up to 77 K).

The investigations conducted and data given in [4] indicate that one of the criteria of assessment of resistance of the welds to hot cracking and porosity is the content of impurity elements, such as oxygen, nitrogen, silicon, sulphur and phosphorus. In addition, the presence of silicon and oxygen in the weld metal of this type affects its toughness and ductility values in a range of cryogenic temperatures. At an oxygen content above a certain critical limit (about 100 ppm) there occurs a dramatic increase in sensitivity of the weld metal to variations in the silicon content. In this case its insignificant increase leads to an increase in the brittle-tough transition temperature and loss in toughness of the weld metal during operation under conditions of cryogenic temperatures. Therefore, maintaining a high purity of the weld metal with regard to the content of impurity elements is one of the conditions for achieving the high operational strength and service reliability of welded joints made in nickel steels using the ferritic filler metal and designed for operation at cryogenic temperatures.

The most efficient method for increasing ductile properties of welded joints is PWHT performed under conditions accepted for steel. This makes it possible to produce structure of tempered martensite with 5 – 8 % residual austenite. The high concentration of the impurity elements in residual austenite provides stability of its parameters at low temperatures. In turn, this prevents initiation and propagation of fracture in the weld metal. However, this method is unsuitable for construction of large isothermal tanks. Therefore, increasing ductility and toughness of the welds at cryogenic temperatures by using approaches which provide stabilization of residual austenite is still a challenge.

Production of a high-purity (with regard to the content of impurities and gases) initial billet for the manufacture of welding wire does not guarantee purity of the weld metal and, thus, the required level of its mechanical properties. Chemical analysis of the metal conducted at different stages of the process of

Table 1. Chemical composition of the materials used

Material	Heat No.	Content of elements, wt.%									
		C	Si	Mn	Ni	Mo	S	P	O	N	H
Steel 0N9	–	0.066	0.18	0.70	8.30	–	0.010	0.003	0.0046	0.0063	0.00004
Wire	8144	0.010	0.05	0.27	11.80	0.10	0.001	0.003	0.0050	0.0010	0.00001
Sv-ON12VI	1B8155	0.016	0.02	0.16	12.74	0.39	0.004	0.010	0.0790	0.0019	0.00001

commercial manufacture of wire showed a substantial increase in the content of impurities (especially silicon and oxygen) during drawing (Figure 1). Metallography of transverse sections of the wire reveals that drawing at the high temperature and deformation values is accompanied by diffusion of the elements, which are part of the composition of scale, into the bulk of the metal.

The control experiment conducted at PWI provided for reproducibility of all stages of the commercial technology for production of the ferritic welding wire, as well as extra operations for cleaning of the surface after each stage of drawing, such as needle milling after rolling, etching of the wire after each drawing stage and mechanical cleaning of the surface after the final stage.

The wire produced as a result of the control experiment met requirements imposed on materials of this grade (Table 1, heat No.8144).

Properties of metal of the welds made by argon-arc welding using the developed wire as the filler correspond to properties of the base metal (Table 2).

The commercial technology for the manufacture of the ferritic welding wire included also the extra operations of preliminary cleaning of the billet after rolling and final machining of the wire surface. As a result, the commercially manufactured wire of the Sv-ON12VI grade (heat No.1V8155) had chemical composition as given in Table 1. The level of impurities in this case is much in excess of that in the wire intended for the control experiment.

Analysis of the data of preliminary investigations into the application of the commercially manufactured

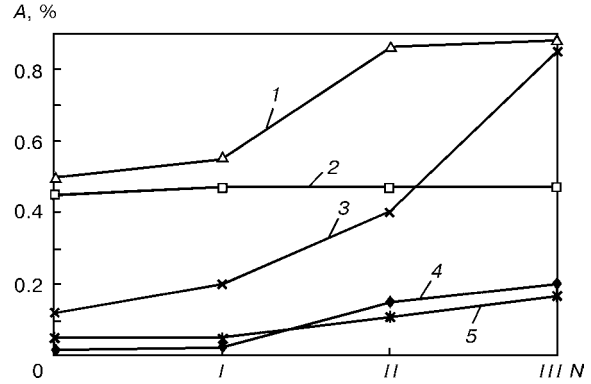

Figure 1. Variation in the amount A of the impurity elements at different stages N of the process of manufacture of welding wire: *0* — initial billet; *I* — rolling to a diameter of 8.0 mm; *II* — drawing to a diameter of 3.0 mm; *III* — drawing to a diameter of 1.6 mm; *1* — [P]·10^{-2}; *2* — [S]·10^{-2}; *3* — [O]·10^{-1}; *4* — [Si]; *5* — [N]·10^{-1}

wire of the Sv-ON12VI grade showed that full strength and sufficiently high toughness and ductility values of the ferritic weld metal could be achieved by improving the welding method and eliminating the effect of residual magnetization of steel welded.

Investigation of magnetic effects in welding of steel with 9 % Ni and a high level of residual induction, performed by using the austenitic filler materials, made it possible to establish a dramatic increase in the gas (oxygen, nitrogen) content of the welds [5]. This was caused by disturbance of gas shielding in argon-arc nonconsumable-electrode welding as a result of form changes and displacement of the arc under the effect of the external magnetic field of the elements being welded.

Investigation into weldability of the magnetized samples of steel ON9 enabled detection of the effect of different factors (structural-technological) on the quality of the welds of the ferritic type, as well as working out of recommendations for ensuring maximum degassing of the weld metal at the stage of a molten weld pool, minimum sensitivity of the arc to variations in the external magnetic field (short or immersed arc) and multilayer gas shielding of the welding zone.

Based on the results of welding of the magnetized elements of steel ON9, the process was carried out using a nonconsumable electrode in argon with the Sv-ON12VI wire used as the filler at a heat input of 18 – 35 kJ/cm (arc voltage — 11 V). A device intended for blowing the root and high-temperature region of the weld with argon was used to eliminate ingress of air, and an extra concentric nozzle was utilized to compress the internal gas flow which directly shields the arc. Analysis of the quality of the resulting welded joints showed that this shielding provided conditions for degassing of the weld pool.

The use of the short-arc method with a high current density eliminates the effect of residual magnetization of the edges on the weld shape.

It was established that in the case of using both commercial and control batches of the wire the weld metal had strength equal to that of the base metal and high values of toughness and ductility over the entire range of test temperatures (Table 2).

Mass of the filler metal deposited in one pass is very important for the level of toughness and ductility. Its increase leads to a variation in the volume of the weld pool, temperature gradient in it, decrease in overheating and, therefore, deterioration in degassing

Table 2. Mechanical properties of welded joints in ON9 steel grade 16 mm thick made in accordance with the developed technology

Filler type	T_{test}, *K*	*Weld metal*			*Welded joint*		
		$\sigma_{0.2}$, *MPa*	σ_t, *MPa*	δ, %	σ_t, *MPa*	$KCV_{w.m}$, MJ/m^2	KCV_{HAZ}, MJ/m^2
Sv-ON12VI	293	594	862	17.3	777	1.81	1.00
(heat No.8144)	77	1018	1188	16.7	1088	1.30	0.88
Sv-ON12VI	293	904	912	16.7	819	0.98	1.04
(heat No.1V8155)	77	1159	1219	15.7	1219	0.67	0.72

Note: Minimum values of the results of not less than three tests at each temperature are given.

conditions. If for the control batch this factor does not have a fundamental effect on the quality of the weld metal, for the commercial batch of the wire an increase in the amount of gases in the weld metal (Figure 2), which at a deposition coefficient of 10 g/(A·h) leads to porosity, is intolerable.

A decrease in the deposition coefficient leads to the necessity to increase the quantity of passes, which involves changes in heat treatment of the previous passes under the effect of the repeated cycle of heating–cooling for the next passes.

To investigate the effect of the technological aspects and procedure of welding on low-temperature toughness and ductility of the weld metal with a ferritic structure, welding was performed on plates of steel the ON9 grade 500 × 300 × 14 and 500 × 300 × × 24 mm in size at a V-groove preparation (included angle — 60°) and heat input of 40 kJ/cm using the commercially manufactured filler wire of the Sv-ON12VI grade. The level of residual magnetic induction of the samples was $11 \cdot 10^{-3}$ T. The specially developed extension devices were used to shield the weld metal and welding zone.

It was established [6] that toughness of the ferritic weld metal depended first of all upon the amount of the residual stable austenite formed in multiple thermal cycles of welding. If the thermal cycle of welding previous passes creates conditions for tempering in the previous welds, i.e. heating temperature is somewhat lower than temperature A_{c_1} (for the ON12 weld $A_{c_1} = 873$ K), residual austenite is formed in an amount of 8 %, which corresponds to its content of steel ON9 and provides the preset level of toughness up to a temperature of liquid nitrogen.

To find correlation between the low-temperature toughness of the weld metal made using the ferritic wire on steel ON9 and the quantity of passes (or the deposition coefficient), Charpy notched specimens for impact toughness tests were cut out from the welded joints at different distances from the weld root, i.e. specimens were made from metal of different passes of the same weld. Schematic of cutting out of the specimens is shown in Figure 3. Investigations were conducted on the welds made at deposition coefficients of 10 and 5 g/(A·h). The quantity of passes in the first case for metal thickness of 24 mm was 9 and 14 mm — 6, while in the second case for 24 mm it was 18 and for 14 mm — 12.

Analysis of results of mechanical tests (Figure 4) showed that the process of welding with a higher deposition coefficient (smaller number of passes) fails to ensure the required level of toughness in the case of using the commercial wire Sv-ON12VI. An increase in the number of cycles of reheating–cooling in the case of using the welding procedure with a low deposition coefficient (5 g/(A·h)) allows stabilization of residual austenite in the weld metal and provides the level of low-temperature ductile properties in excess of the permissible values for the base metal (Figure 5). For a final pass, in order to create the required conditions for stabilization of residual austenite, which guarantees the high value of impact toughness, it is necessary to use an additional arc remelting without a filler wire at a low heat input (not more than 6 kJ/cm).

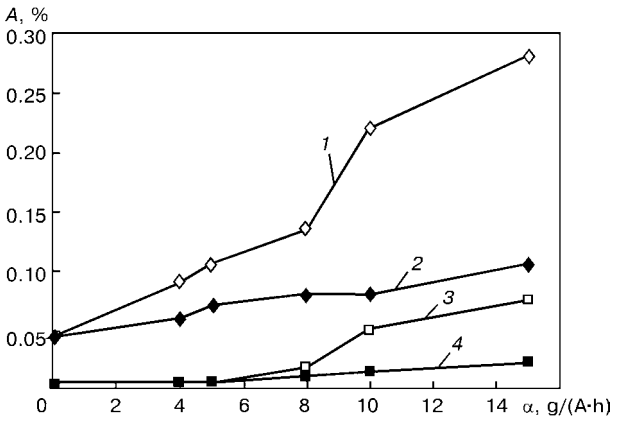

Figure 2. Effect of deposition coefficient α on variations in the gas content of the weld metal, %: *1* — $[N] \cdot 10^{-1}$; *2* — $[N]_c \cdot 10^{-1}$; *3* — $[O]$; *4* — $[O]_c$

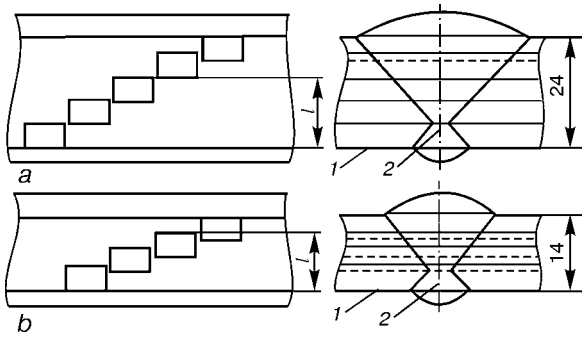

Figure 3. Schematic of cutting out of specimens from experimental joints in steel ON9 24 (*a*) and 14 mm (*b*) thick: *1* — baseline plane; *2* — notch line; *l* — distance of the location of cutting out of specimens from the baseline plane

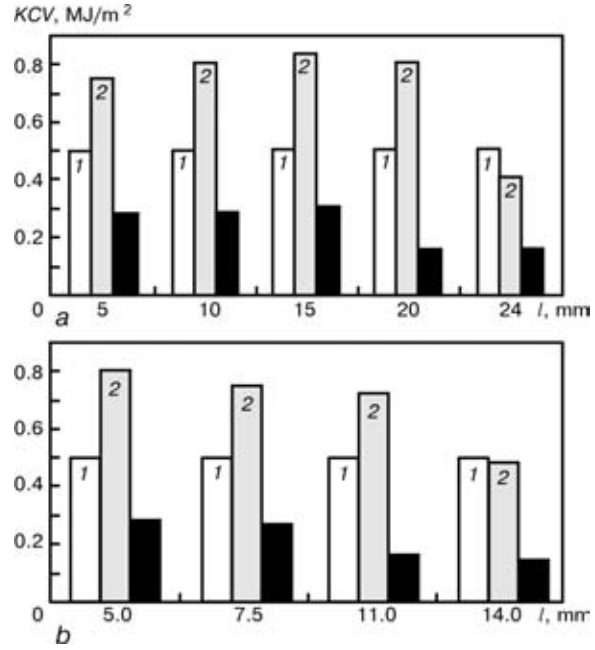

Figure 4. Variation in impact toughness *KCV* across the section of a welded joint at T_{test} = 77 K depending upon the deposition coefficient α = 5 (*2*) and 10 g/(A·h) (*3*) at metal thickness 24 (*a*) and 14 mm (*b*); *1* — KCV_{BM}

The principle of reheating–cooling is most completely utilized in multipass welding with stringer welds using a short or immersed arc and by feeding the wire to the leading portion of the weld pool.

Fractography of fractures proved transition from tough to quasi-brittle fracture of the ferritic weld

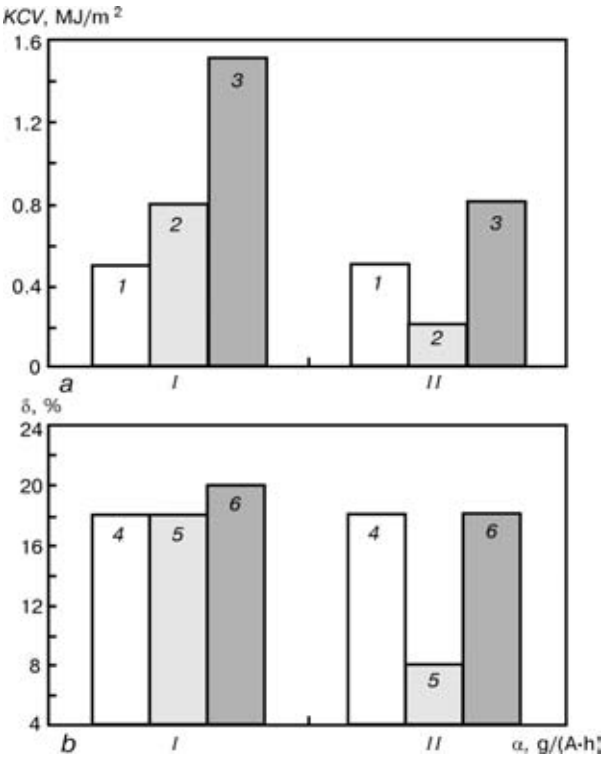

Figure 5. Variations in ductile properties of welded joint in ON9 steel grade 24 mm thick depending upon the deposition coefficient at 77 K: *a* — impact toughness; *b* — elongation; *I* — α = 5; *II* — α = 10 g/(A·h); *1* — KCV_{BM}; *2* — *KCV*; *3* — KCV_r; *4* — δ_{BM}; *5* — δ; *6* — δ_r

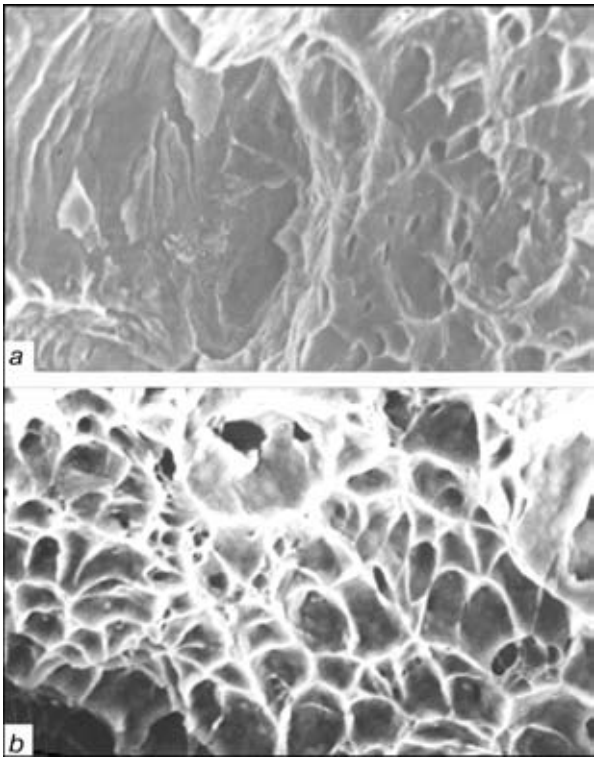

Figure 6. Effect of deposition coefficient α on morphology of fracture of ferritic welds at 77 K: *a* — α = 5; *b* — α = 10 g/(A·h) (×1500)

metal in welding with a deposition coefficient of 10 g/(A·h) (Figure 6).

CONCLUSIONS

1. The investigations conducted made it possible to produce full-strength welded joints with a high level of toughness and ductility at temperatures of up to 77 K in welding steels with 6 to 9 % Ni.

2. Welding wire of the ferritic Sv-ON12VI grade was developed.

3. To ensure low-temperature toughness of the weld metal produced by using the Sv-ON12VI wire, it is necessary to create conditions for tempering of the metal after each welding pass. It is recommended to use a short arc with a limited deposition efficiency (α ≤ 5 g/(A·h)) and an increased shielding from air. The weld metal should contain about 5 – 8 % residual stabilized austenite.

REFERENCES

1. Tharby, R.H., Heath, D.J., Flannery, J.W. *et al.* (1978) Welding 9 % Ni steel. A review of the current practices. *Australian Welding J.*, **2**, 11 – 18.
2. Otsuka, H., Abiko, N., Fukuhara, J. *et al.* (1979) Automatic TIG used for 9 % nickel steel storage tanks. *Welding and Metal Fabrication*, **4**, 239 – 240, 242 – 245.
3. Minehisa, S., Nagai, A., Shirane, Y. *et al.* (1978) Welding of 9 % nickel steel. *Hitachi Zosen Technical Review*, **2**, 140 – 146.
4. Agusa, K., Kosho, M., Nishiyama, N. *et al.* (1986) Production of 9 % Ni steel UOE pipe with ferritic filler. *Transact. of Iron and Steel Inst. of Japan*, **5**, 359 – 366.
5. Yushchenko, K.A., Pestov, V.A., Starushchenko, T.M. *et al.* (1991) Magnetic phenomena in welding steel ON9. *Avtomaticheskaya Svarka*, **10**, 56 – 58.
6. Tamura, H. (1980) Residual austenite and impact toughness on the heat-affected zones at repeated welding cycles in steel with 9 % Ni. *Yosetsu Gakkaishi*, **49**, 854 – 860.

EXPERIENCE OF APPLICATION OF ARC SURFACING WITH A PULSED FEEDING OF ELECTRODE WIRE

V.A. LEBEDEV, A.E. KOROTYNSKY, V.M. MOZOK and **V.G. PICHAK**
The E.O. Paton Electric Welding Institute, Kyiv, Ukraine

ABSTRACT

Experience gained in restoration of a number of complicated civil engineering objects of Ukraine by the methods of the mechanized arc surfacing using a pulsed feeding mechanisms based on quasi-waved transducers with controllers of electrode wire pulsed feeding parameters, is analyzed. Long-time operation of this type of mechanisms proved their high performance and reliability. It has been revealed that the use of mobile systems, such as a semi-automatic machine with a pulsed feeding — a small-sized arc power supply source, is promising. Special designs of resonance AC arc power sources can be used as a latter for these systems.

Key words: *surfacing, semi-automatic machine, power source, feeding mechanism, pulse, feeding, electrode wire, manufacture, object, deposited layer, quality, efficiency*

The arc mechanized surfacing, one of basic technologies realized with the help of the semi-automatic machines, is widely used for restoration and strengthening of assemblies and parts of different manufacturing mechanisms, transport means, road machinery and production and processing equipment. The surfacing is especially effective with use of self-shielding flux-cored electrode wires which impart purposefully the definite properties. The wide spreading of the mechanized surfacing is due to some basic circumstances:

- significant increase in service life of assemblies and parts at relatively small material and energy consumption;
- use of equipment and materials under different working, climatic and environmental conditions for a wide range of objects of restoration and strengthening, manufactured of different metals and having various shapes of the surface treated;
- mobility of equipment and low requirements to the skill of operators.

In spite of the above-mentioned advantages, this process needs improvements both concerning equipment for its realization and also from the point of view of some (rather important) technological aspects. These works are constantly carried out by the specialists of the E.O. Paton Electric Welding Institute. The results of this work are implemented, as a rule, at different enterprises of the national economy.

The present work is aimed at the study of results of using a pulsed feeding of the electrode wire, in particular self-shielding flux-cored wire, in restoration and strengthening surfacing.

The feeding of the electrode wire in arc mechanized process, realized with pulses of frequency of the order of tens of hertz, is described in [1]. This process, in shielded-gas welding in particular, is continued to be studied at the present time.

Mechanisms of a pulsed feeding, used in the mentioned process, are based on reducer-free transducers of movement of the electrode wire using single-sided clamps. For solid steel and aluminium electrode wires the use of these technical solutions was feasible in a number of cases, in particular for research works. However, they are not sufficiently reliable and have a small service life for industrial implementation or for realization of a large volume of single jobs. In addition, these systems of a pulsed feeding of the electrode wire are almost unsuitable for the flux-cored wires due to great changes in a preset pitch of feeding at deformation of their sheathes which can lead even to the damage of the latter.

Now, the new designs of pulsed feeding mechanisms have appeared on the basis of quasi-wave transducers (QWT). Their propellers are the conventional pairs of feeding and pressure rollers that can realize the pulsed movement of easily-deformed electrode wires to which the self-shielding flux-cored surfacing electrode wires belong. This makes it possible to develop and use a number of pulsed feeding mechanisms with QWT in the arc mechanized equipment for surfacing jobs. The main characteristics of the designed mechanisms are the design solution of relations between frequencies of a pulsed feeding and their pitch. This problem was solved by a selection of a gear ratio of the reducer with QWT and diameter of a feeding roller in accordance with recommendations given in [2]. This work was an integral part of investigations of effect of a pitch of the pulsed feeding of the flux-cored wire on geometric sizes of the deposited beads, mechanical characteristics of the deposited metal and its composition. The pulsed feeding mechanisms of the designed series were mounted in a basic model of the semi-automatic machine PSh107V [3], having the necessary feed back systems, installed into an adjustable electric drive, including those by the arc process parameters, which can provide the stabilizing effect on the surfacing, performed, as a rule, with an increased electrode wire stickout. It should be noted that a driven electric motor DPU87-

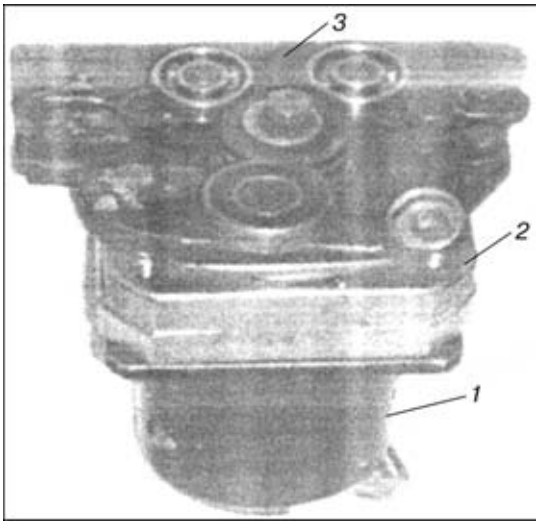

Figure 1. Mechanism of LM type with QWT for a pulsed electrode wire feeding: *1* — electric motor; *2* — mechanism with QWT; *3* — device of feeding and pressing of electrode wire, consisting of elements of QWT output shaft unloading

75 of the semi-automatic machine PSh107V was used for some mechanisms of a pulsed feeding, while for others mechanisms the electric motors were different. Such choice was explained by the necessity in use of the mechanisms of a pulsed feeding with a large gear ratios. In the given case a rated frequency of rotation of the DPU87-75 electric motor shaft can be not sufficient to obtain the required integral speed of feeding the surfacing electrode wire. In the illustrated design of the pulsed feeding mechanism a device [4] was used which unloads its output elements. Thus, the basic model of the semi-automatic machine PSh107V was provided with one more modification, specially designed for a realization of surfacing with self-shielding flux-cored electrode wires at their controllable pulsed feeding. This modification of the semi-automatic machine has a design index PSh107R. It can be used with any arc power source of suitable characteristics of the output parameters (current and voltage). It should be noted that the process of surfacing with the pulsed feeding of the self-shielding flux-cored surfacing electrode wires is characterized by a considerable decrease in level of the surfacing current as compared with that used in stationary modes, thus widening its capabilities, in particular, in strengthening or restoration of thin-sheet metal structures, for example, the cultivator tooth, etc. For example, if the lower limit of surfacing current is 280 – 290 A for flux-cored wires of 2.8 – 3.2 mm diameter under the stationary conditions, then, when the pulsed feeding is used it is 140 – 170 A. In addition, the level of surfacing voltages can also be somewhat decreased even in case of using the increased stickout of the electrode wire. Here, the arc power sources of the simplest designs are used in the process of surfacing, i.e. those, which have no stabilization of the output voltage. These are conventional rectifiers with the help of which the high characteristics of the process stability without free oscillations typical of the processes with an increased stickout of electrode can be obtained in a pulsed feeding of the electrode wire [5].

The experience of industrial application of the semi-automatic machines with a pulsed feeding of the electrode wire is high enough now by the amount of both deposited metal and the objects of application [6]. The most objects of the sugar and mining industries were subjected to the restoration using the methods of arc surfacing with a pulsed feeding of the electrode wire. All the works on restoration made at these enterprises, even in emergency situations, were economically efficient. Two types of quasi-wave mechanisms of a pulsed feeding, LM-50 and LM-78, having a gear ratio 50 and 78, respectively, and also a system of feeding rollers, which provides definite pitches of feeding, were developed for a restoration surfacing. Moreover, both mechanisms were equipped with controllers of a pulse shape, with the help of which the parameters of movement of the electrode wire in a pulse can be changed up to its partial reversing, thus providing significant accelerations. Mechanisms of the pulsed feeding of the electrode wire on the base of QWT of LM-50 and LM-78 types are given in Figure 1.

The present work describes several typical examples of fulfilment of surfacing works using a pulsed feeding of the electrode wire.

Surfacing and welding with solid electrode wires (Parafievsky Sugar Factory). The casing of a diffuser semi-cylinder was subjected to the restoration surfacing. In this case it was impossible to replace the casing by new sheets because of the peculiarities of the design of the diffuser itself. The thickness of the casing metal was 8 mm, the rejected thickness — 5 mm and allowable thickness after repair — 6 mm. About 50 mm^2 area was subjected to restoration. First two semi-automatic machines A-547Um with 1.2 mm diameter electrode wire Sv-08G2S (C — 0.11; Si — 0.5; Mn — 1.4; Cr ≤ 0.1 wt.%) were used in the technological process. Then, the semi-automatic machines with pulsed feeding mechanisms LM-50 and LM-78 of feeding pitches of 2.50 and 1.41 mm in a pulse, respectively, of 1.6 mm diameter electrode wire Sv-08G2S were used, because some works could not be fulfilled with semi-automatic machines A-547Um. In both cases the same arc power supply source VDU-506 at some schematic modifications of semi-automatic machines A-547Um was used. Regions of single- and multi-layer surfacing were made. Thus, it was possible to compare the results of surfacing using different feeding mechanisms (stationary and two pulsed mechanisms with different parameters) under the real industrial conditions (Table).

In surfacing with semi-automatic machines A-547Um, 12 cylinders with CO_2 were consumed for 100 kg of electrode wire Sv-08G2S. The same amount of CO_2 was used in surfacing with semi-automatic machines with mechanisms LM-50, LM-78, but, here, for 500 kg electrode wire Sv-08G2S of 1.6 mm diameter. This is explained by a lower consumption of CO_2

Application of semi-automatic machines with different types of mechanisms of a pulsed electrode wire feeding in restoration of a diffuser casing

Type of mechanism	*Kind of feeding*	*Works performed*	*Conditions of welding and surfacing performance*	*Surfacing conditions*	*Results of experiments*
A-547Um	Stationary	Surfacing of thicknesses of more than 4 mm, welding of structure elements	In flat and vertical positions	180 – 210 A 26 – 28 V	About 10 m^2 were deposited. There are lack of penetration and spatters of large drops of electrode metal, thus requiring their removal with an abrasive tool
LM-78	Pulsed with 1.41 mm pitch	Surfacing of thicknesses of less than 4 mm, welding of structure elements	In flat, vertical and semi-overhead positions	180 – 210 A 24 – 28 V	About 15 m^2 were deposited. There are separate places with a lack of penetration. No spattering of electrode metal. The oxide dust deposit is easily removed by a soft steel brush
LM-50	Pulsed with 2.50 mm pitch. Reverse in pulse up to 12 % from the pitch length	Surfacing of thicknesses of less than 3 mm, including also the multilayer surfacing without cleaning	Same	160 – 180 A 24 – 28 V	About 25 m^2 were deposited. No claims to the quality of deposited metal. The easy arc exiting was noted additionally (from one or, sometimes, two short circuitings)

Note. VDU-506 was used as a power source.

in the processes with a pulsed feeding in positions different from the flat position, and also by an extra consumption of CO_2 for process stabilizing (there are «shooted» and welded stickouts of the electrode wires) with the semi-automatic machine A-547Um, non-efficient operations on surfacing of poorly formed areas and so on.

Surfacing with self-shielding welding flux-cored wires (North Ore-Dressing Plant, Krivoj Rog). The restoration of a casing of a cone-type 48 t crusher was made. To fulfil surfacing, 600 kg of 2.8 mm diameter PP-AN7 (C — 0.09 – 0.12; Si — 0.3 – 0.4; Mn — 0.9 – 1.2; S — up to 0.02; P — up to 0.02 wt.%; Fe — balance) and 3.0 mm diameter PP-AN1 (C — 0.09 – 0.1; Si — 0.07 – 0.15; Mn — 0.6 – 0.8; S — up to 0.03; P — up to 0.03 wt.%; Fe — balance) electrode wires were consumed. All the volume of surfacing jobs was performed using the semi-automatic machine with LM-50 mechanism and arc power source VS-632 at 160 – 180 A. In this case the position of the surface deposited (flat with 30° inclination and vertical) did not present any difficulties for an operator, transition from one type of the surface to another was made without an additional adjustment of the surfacing conditions. The wear of the surfaces deposited was within 14 – 30 mm. Time, spent for this element of surfacing, was three days at three-shift work.

The second operation at the same casing was the restoration of a seat for a bushing-insert of 600 mm diameter and 1100 mm length. Wear was, on average, 2 mm for a diameter. The same equipment was used. The total time of surfacing was 4 days, and one-day additional time for the mechanical treatment of the seat.

Calculation of the total expenses for the restoration of the casing showed that they are 2.9 times lower than those spent for purchase of the new casing. The service life of the restored casing was not reduced.

Surfacing with self-shielding surfacing electrode wires (South Ore-Dressing Plant, Krivoj Rog). Teeth of shafts-gears of the drive of crushing mills with the following parameters were subjected to surfacing: number of teeth — 19, pitch — 25, length and inclination of a tooth relative to the axis of shaft-gear are 480 mm and 17°, respectively; material — steel 40Kh (C — 0.4; Cr — 1.0 wt.%; Fe — balance). Unlike the previous examples, in this case it was necessary during restoration of teeth to provide the appropriate mechanical properties of the deposited layer both by using surfacing electrode wires and also as a result of the restoration technology used. The self-shielding surfacing wire of 3.2 mm diameter was used which could provide the following parameters of the deposited layer of metal:

- ultimate strength — 850 – 900 MPa;
- impact strength of 90 J/cm^2 at temperature +20 °C (not less) with a Mesnager notch;
- elongation — 20 % (not less).

In addition, the surface deposited should have minimum tolerances for post mechanical treatment.

Using the semi-automatic machine of a basic model PSh107V with arc power source BS-600m it was impossible to provide the required density of metal, shape of the deposited bead and its mechanical properties. Moreover, the current of the arc process was 250 – 280 A even at its steady proceeding, and the share of the parent metal in the deposited bead was sufficiently high. It is evident in this case that the energy input during surfacing is excessive.

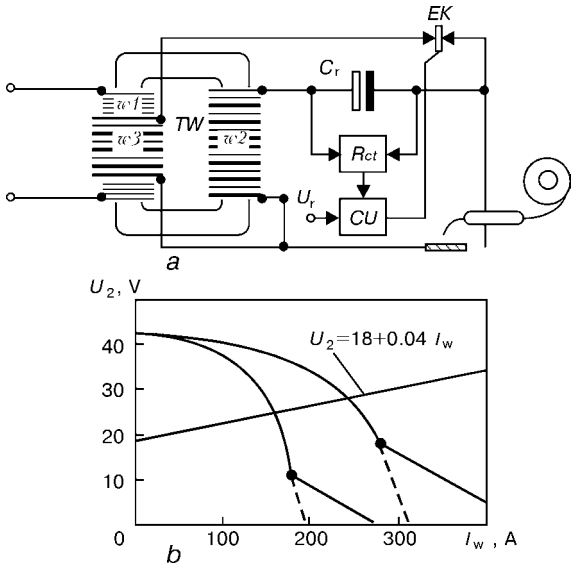

Figure 2. Schematic diagram of AC arc power source (*a*) and volt-ampere characteristics of power source and welding arc (*b*)

It was possible to provide the required quality of the restored teeth by using a modified version of the semi-automatic machine PSh107R with a feeding mechanism of LM-50 type, having 2.2 mm feeding pitch and a reversing movement of the wire in a pulse up to 10 % of the pitch length. The worn-out side of the tooth was surfaced with longitudinal beads from a root to a point of the tooth with auxiliary transverse oscillations of the electrode wire, thus providing overlapping of bead edges using current of 170 – 200 A. The quality of the deposited layer corresponded to the that of the initial metal by the mechanical properties and appearance.

We had an opportunity to carry out the additional examination of deposited teeth, when the mill after its twice service life was dismantled because of the reconstruction of the shop. It appeared, that the wear of the deposited surfaces of the teeth was 3.5 times less than that of the gear teeth supplied from the customer. The analysis of the economical efficiency of the offered and realized technology of restoration of the shaft-gear teeth showed that it can be profitable even in case of providing equal service properties of the restored and supplied shafts-gears by the customer.

Separate examples showed that the tasks of restoration of assemblies and parts of machinery of various complexity can be solved by using the semi-automatic machines with a pulsed feeding of the electrode wire rather effectively and qualitatively also in those cases when their fulfilment is impossible or difficult. The offered high reliability of systems of a pulsed feeding of the electrode wire is confirmed on the basis of QWT. The design of the semi-automatic machines of PSh107 type allows its easy adaptation for operation with any arc power sources, existing at the enterprise.

It should be specially noted that for the processes of surfacing with a pulsed feeding of the electrode wire it is sufficient to use the AC arc power sources of all the types which are usually used for realizing manual arc processes, i.e. conventional welding transformers with falling external characteristics and controllers of current of almost any types. In this case, as the experience showed, the basic requirements to the transformer consist in providing a sufficient capacity and required short-circuit current. This technical solution can be rather useful if the surfacing is performed at the enterprises and objects where only arc power sources for the manual arc welding are in service. In addition, it is evident that the welding transformers are much simpler, cheaper and reliable, than the rectifiers, for the arc mechanized processes. We used the complexes, a semi-automatic machine with a pulsed electrode wire feeding — welding transformer, in particular for surfacing of scrolls of a suction-tube dredger directly on the object if the transformer for the manual arc welding was included into a repair complex of the object. In this case the systems of control and adjustment of the semi-automatic machine PSh107R were equipped additionally with a power source connected to the welding transformer output.

There is a large scope of works on the restoration and strengthening which are realized using the mechanized arc equipment including that with a pulsed electrode wire feeding, where a mobile set of an automatic machine–arc power source is required.

The most promising direction for the mechanized processes of AC welding and surfacing is a use of resonance of voltages in the secondary circuit of the power source, characterized by high energy-saving properties and small mass-dimensional characteristics [7]. However, due to a low short-circuit current (as compared with traditional power sources) the direct use of the resonance sources encounters some difficulties. The measures should be taken for increase in the short-circuit current at the moment of electrode metal drop transition to a molten pool.

Diagram of one of possible versions of the AC arc power source is presented in Figure 2, *a*. The power source consists of a core-type welding transformer *TW* with a supplying winding *w1*, located at the first core. The winding *w2*, whose leakage inductance together with a capacitive reactor C_r forms a resonance circuit, is located at the second core. The device is featured by a winding *w3* which forms a close inductive coupling with winding *w1*.

Figure 2, *b* presents external characteristics of the arc power source with a volt-ampere characteristics of the welding arc. At the moment of transition of the drop and abrupt reduction in arc voltage the voltage at the reactor is increased. This signal, taken from C_r, enters the output of the rectifier *Rct* and used in the control unit *CU* for the formation of a command of switching on of a contactless key *EK* made on a triac. Thus, the short-circuit current addition is provided.

These power sources in a set with semi-automatic machines, having systems of a pulsed electrode wire feeding, were tested during fulfilment of some sur-

facing jobs under the real industrial conditions. Test results make it possible to conclude that the complex, a semi-automatic machine with a pulsed electrode wire feeding — a resonance AC arc power source, which provides a required level of the short-circuit currents, can be a basis for the creation of mobile mechanized equipment for restoration and strengthening of assemblies and parts, including those used under the conditions differed from the shop conditions. It should be noted that in use of QWT instead of a traditional feeding mechanism it is possible to decrease twice the set power of the power source (of any type for the same diameter of the wire).

CONCLUSIONS

1. One of the most effective methods of widening the feasibility of arc methods of restoration and strengthening of different-purpose machine parts is the use of controllable pulsed feeding mechanisms based on QWT, having high reliability, simple in design and not requiring special conditions in service and maintenance, in the arc mechanized equipment.

2. Creation of mobile complexes, a semi-automatic machine — a small-sized power source with the use of special designs of resonance AC arc power sources, is an additional reserve.

REFERENCES

1. Voropaj, N.M. (1996) Parameters of conditions and technological capabilities of arc welding with a pulsed feeding of electrode and filler wire. *Avtomaticheskaya Svarka*, **10**, 3 – 9.
2. Lebedev, V.A. (1996) Control of speed and pitch in a pulsed feeding of electrode wire in mechanisms based on a quasi-wave transducer. *Ibid*., **6**, 34 – 37.
3. Lebedev, V.A., Moshkin, V.F., Pichak, V.G. (1998) Semiautomatic machines of a single modular design for welding, surfacing and cutting. *Svarochnoye Proizvodstvo*, **1**, 24 – 28.
4. Mozok, V.M., Lebedev, V.A., Pichak, V.G. *et al*. *Feeding mechanism*. SSSR author's certificate **1771903**, Int. Cl. B 23 K 9/12. Publ. 30.10.92.
5. Lebedev, A.V., Suprun, S.A. (1978) Effectiveness of stabilizing of a mean value of current in semi-automatic welding. *Avtomaticheskaya Svarka*, **10**, 37 – 41.
6. Mozok, V.M. (1996) Improvement of technology of welding and surfacing with consumable electrode using a mechanical modulator of welding current. *Ibid*., **2**, 57 – 58.
7. Lebiediew, W.K., Korotynski, A.E., Zuk, G.W. (1997) Some properties of arc welding processes supplied by power sources with LC resonant circuits. *Biuletin Instytutu Spawalnictwa w Gliwicach*, **3**, 34 – 37.

PECULIARITIES OF WELDING THIN-SHEET LOW-CARBON STEELS USING A PULSED-PERIODIC RADIATION OF CO_2-LASER

V.Yu. KHASKIN, S.Yu. PAVLOVSKY, V.P. GARASHCHUK, V.D. SHELYAGIN and **E.I. GONCHARENKO**
The E.O. Paton Electric Welding Institute, NASU, Kyiv, Ukraine

ABSTRACT

It is shown that welding of low-carbon steels using radiation of CO_2-laser in a pulsed-periodic mode (PPM) produces more narrow and deeper welds that in a continuous mode at a power of radiation equal to an average power of PPM. At optimum frequency of pulses the structure of the weld root part becomes more regular, the HAZ width is decreased, overheating (coarse-grained) region is either absent or becomes not clearly defined.

Key words: *laser welding, CO_2~-laser, continuous radiation, pulsed-periodic radiation, low-carbon steels, geometry of welds, strength, structure*

Low-carbon sheet steels are used in industry for different structures (manufacture of bodies of motor transport, instruments, etc.) [1]. Therefore, the problems of the producing high-quality permanent joints from these steels are actual. In many case it is necessary to produce continuous welds whose metal is equal in strength to the parent metal. In addition, the weld should have a good appearance, minimum residual stresses and strains in the structure welded, and also minimum width of weld and HAZ [2].

One of the most efficient and precision methods of fusion welding, providing the high quality, is a laser welding [3]. It can be performed both by a continuous and pulsed-periodic radiation [4]. Both modes of radiation can be generated by solid-body and gas CO_2-lasers. At present the powerful CO_2-lasers, generating a continuous radiation, are widely spread in industry due to a higher efficiency factor and low cost of consumables [5].

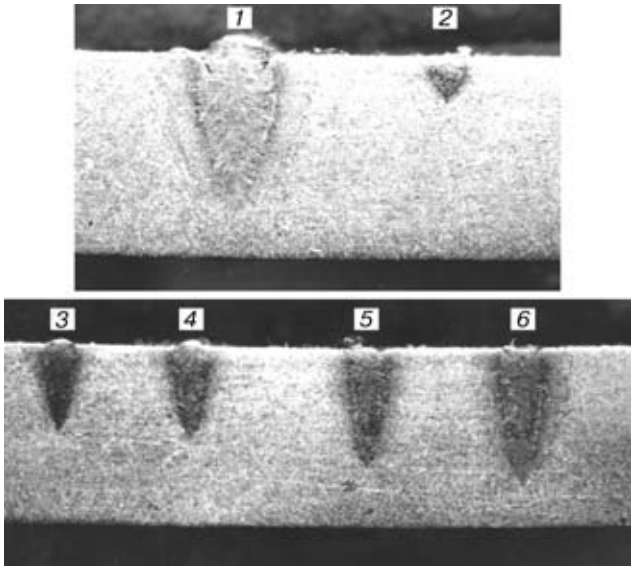

Figure 1. Macrostructure of transverse section of penetration in steel 15rm (δ = 10 mm, v_w = 18 m/h) at a continuous radiation (No.1 — P_{cont} = 4.85 kW, No.2 — P_{cont} = 1.4 kW) and at a pulsed-periodic radiation with f = 330 Hz (No.3 — $P_{av.pulse}$ = = 1.55 kW, G = 3; No.4 — $P_{av.pulse}$ — 1.96 kW, G = 2.5; No.5 — $P_{av.pulse}$ = 2.54 kW, G = 2; No.6 — $P_{av.pulse}$ = 3.4 kW, G = 1.5)

The present work was aimed at a comparative investigation of geometry, strength and structure of welds made by the continuous and pulsed-periodic radiation of CO_2-laser on low-carbon steels (08rm, 10rm and 15rm (rimmed)). Experiments were performed in technological laser of the LT-104 type of a high-frequency pumping [6]. Radiation relative to fixed samples welded was displaced with the help of a two-coordinate programmable manipulator. The zone of action of the laser radiation was protected in all the cases by CO_2.

For the preliminary selection of conditions of welding low-carbon steels using a pulsed-periodic radiation, a number of welds was made on sheet hot-rolled samples of δ = 1, 3, 5 and 10 mm. Here, the welding speed v_w was 18, 36 and 72 m/h, radiation was focused by a single-lens objective at a focusing distance F = 300 mm, deepening of focus ΔF under the surface of the sample welded was 0 – 4 mm. All the experiments on study of effect of a pulse duty factor of the PPM on the characteristics of weld metal were performed at the condition $P_{pulse} = P_{cont}$, i.e. the power of a laser radiation in the pulse was the same as that in the continuous mode (CM). In separate cases the experiment was repeated in CM of generation of radiation (G = 1, f = 0 Hz) at power P_{cont} = = $P_{av.pulse}$, where $P_{av.pulse}$ is the average power of radiation in PPM. Ranges of power change were 1.5 – 5.0 kW. Results were obtained from macrosections, etched in iron chloride.

Analysis of results of preliminary experiments (Figure 1) showed that at PMM modulation of CO_2-laser radiation it is possible to produce more narrow and deep welds than at similar CM generation of radiation. The effect of increase in depth of penetration is 20 – 50 %. The weld shape factor is decreased

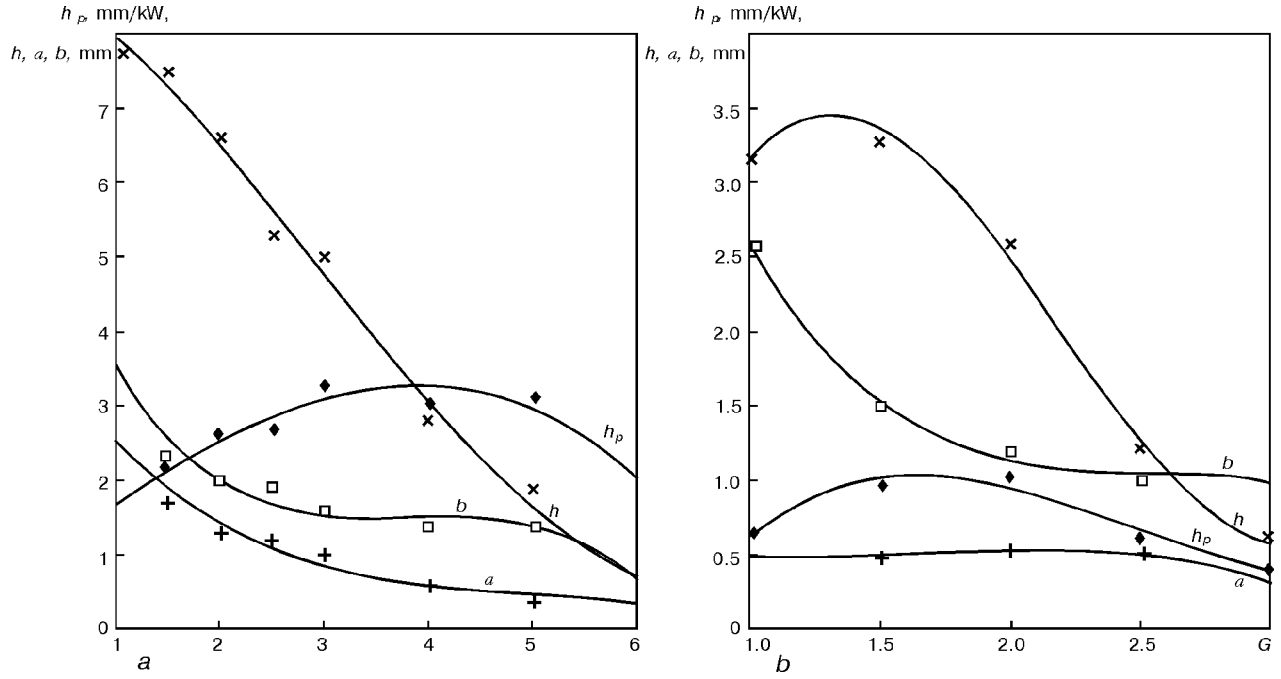

Figure 2. Relationship between parameters h_P, h, b and a (mm) and a pulse duty factor for steel 15rm (δ = 10 mm) at v_w = 18 (*a*) and 72 m/h (*b*)

in this case by 20 – 25 %. With increase in average power of the pulsed-periodic radiation the optimum pulse duty factor is increased (at $P_{av.pulse}$ = 1.9 kW G_{opt} = 1.5; at $P_{av.pulse}$ = 3.0 – 4.4 kW G_{opt} = 2), and optimum frequency is decreased (at $P_{av.pulse}$ = 1.7 – 1.9 kW f_{opt} = 330 Hz; at $P_{av.pulse}$ = 3.0 – 3.1 kW f_{opt} = = 200 Hz), that was confirmed by the results of [4].

It was also established that with increase in the welding speed the HAZ, depth and width of penetrations are decreased at a proportional preserving of configuration. The upper bead (reinforcement) formation is improved. Thus, at low speeds of penetration (18 m/h) using continuous and pulsed-periodic (f = = 330 Hz) radiation the gas pockets of a depth of 10 – 20 % of the penetration depth may occur in the upper part of the weld, and in case of a pulsed-periodic radiation the metal is spattering. At 36 m/h speed these drawbacks are eliminated, and at higher speeds (for example, 72 m/h) a stable formation of the quality bead reinforcement is observed.

Figure 2 shows the dependence of the penetrability $h_P = h/P$, depth of penetration h, width of weld b and HAZ a on the pulse duty factor G for welds made on steel 15rm (δ =10 mm) at the frequency of pulses f = 330 Hz. Experimental results are approximated with an error ± 5 %. Figure 2 indicates that relation $h_P = f(G)$ has a maximum, and values h_P for $G > 1$ (G = 1 corresponds to the continuous mode of radiation) are always higher than those for the continuous mode of radiation.

It is seen from the diagram given in Figure 2, *a* that in case of a low-speed laser welding the maximum penetrability is G = 3 – 5. However, it can be considered that G = 3 will be optimum at minimizing b and a at simultaneous increase of h. In case of a high-speed laser welding (Figure 2, *b*) the optimum is shifted to the side of welding with a continuous radiation and amounts to $G \approx 1.5$.

It follows from the analysis of given experimental results that the position of optimum for the pulse duty factor depends on the power of radiation and welding speed. With increase in power the optimum pulse duty factor is increased, while with increase in welding speed it is decreased.

In case of penetration with a continuous radiation the weld root has a good formation that is described in [3]. In penetration with a pulsed-periodic radiation at frequency f = 330 Hz this shape of penetration becomes more regular and the height of «peaks» is decreased by 3 – 4 times.

From the results of described experiments the following condition parameters were selected for welding in PPM of sheet samples from low-carbon steel (δ = 1 and 3 mm): G = 3, f = 300 Hz, v_w = 36 m/h. Value $P_{av.pulse}$ was selected separately for each of thicknesses welded to produce the quality formation of the weld root.

Three series of experiments on welding in PPM and CM were carried out:

- butt welding and penetration of sheets of 3 mm thick steel 10rm;
- the same, using 1 mm thick steel 08rm;
- overlap welding of 1 mm thick steel 08rm.

Welding was performed in CO_2. In all the cases a through penetration with a good weld root formation was obtained. Conditions of experiments and their results are given in Table. This table indicates also the results of tensile tests performed on standard specimens (GOST 6996–66, types XIII and XXIV) using a universal TsD-4 machine. During fracture the force was measured and then the ultimate tensile strength σ_t was determined from the ratio of area of non-de-

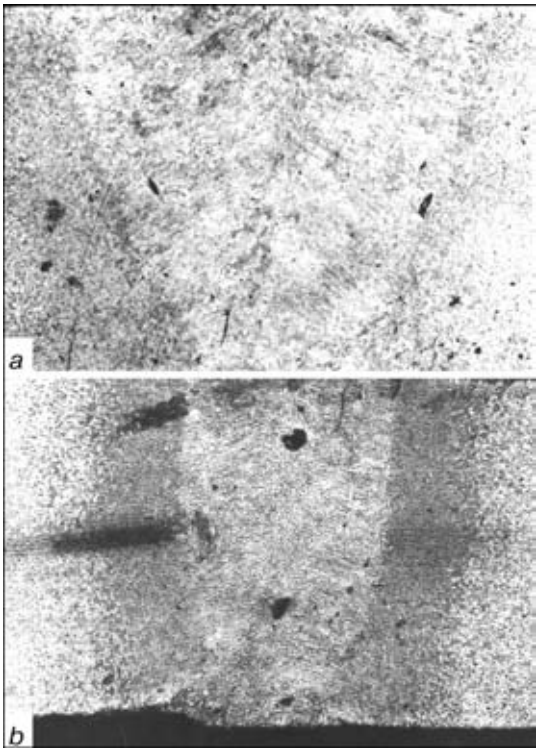

Figure 3. Microstructure of transverse section of weld made on steel 10rm at a continuous (*a*) and pulsed-periodic radiation (*b*) (×25)

formed specimen at the fracture spot to the measured force.

The tests showed that the metal of welds made by the laser welding is equal in strength to the parent metal and sometimes it is even superior to it. Difference in mechanical characteristics of welds made in PPM and CM was observed. It is most clearly manifested for 3 mm thick sheets. The strength of butt joints made by the pulsed-periodic radiation is by 5 – 15 % higher than that of the similar joints made by the continuous radiation.

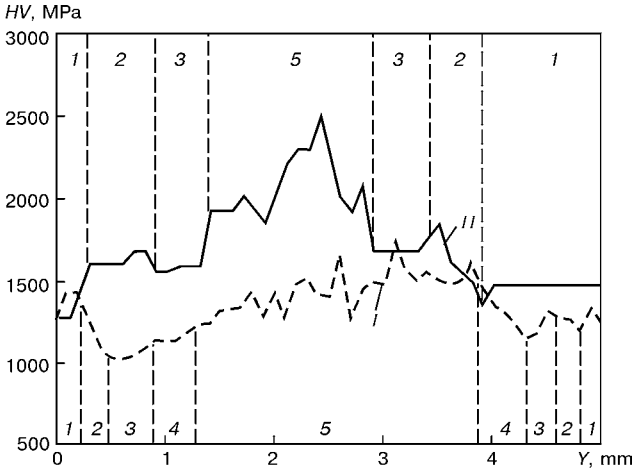

Figure 4. Distribution of hardness *HV* in direction *Y* normal to weld plane, at δ/4 depth in butt welding of steel 10rm (δ = = 3 mm): *I* — continuous radiation (*G* = 1, v_w = 36 m/h, *P* = = 3.22 kW); *II* — pulsed-periodic radiation (*f* = 330 Hz, *G* = 3, v_w = 36 m/h, *P* = 2.2 kW); *1* — parent metal; *2 – 4* — zones of partial recrystallization of fine and coarse grain, respectively; *5* — weld

Conditions of experiments on welding low-carbon steels in PPM (*G* = 3, *f* = 330 Hz) and CM (v_w = 36 m/h)

δ, *mm*	*Type of joint*	*Type of CO_2-laser radiation*	*Radiation power P_{cont} or $P_{av.pulse}$, kW*	*Averaged result of tensile test σ_t, MPa*
3	Butt	Pulsed-periodic	2.20	370
3	Penetration	Same	2.20	380
3	Butt	Continuous	3.22	305
3	Penetration	Same	3.22	360
1	Same	Pulsed-periodic	1.08	355
1	Butt	Same	1.08 – 1.09	395
1	Penetration	Continuous	1.06	353
1	Butt	Same	1.00	–
1	Overlap	»	2.20	340
1	Same	Pulsed-periodic	2.00	300

To examine the microstructure of welds and penetrations, templets of 20 × 15 × δ mm size were cut from the appropriate samples, then they were clamped in mandrels and macro- and microsections were manufactured. The microsections were subjected to cold etching in 4 % alcohol solution of nitric acid during 3 – 5 s. Examination and photographing of microstructures were made in optical microscope Neophot-32 (Figure 3).

Microhardness was measured on etched microsections along the line passed at the depth of δ/4 from weld top in plane, being transverse to the weld axis direction (Figure 4). Pitch of measurements was 0.1 mm at 0.5 N load. Microhardness meter of the M-400 MVK-E type of LECO Company was used.

It was established that in all the cases the parent metal has a ferritic-pearlitic structure with a dominating amount of ferrite. The structure preserves the traces of rolling. Ferritic grain index was 8 and 9 (GOST 5639–82), hardness of parent metal — *HV* 1200 – 1400 MPa.

Samples welded in CM (Figure 3) have a ferritic-pearlitic structure of the weld metal with a precipitation of a hypoeutectic ferrite along the boundaries of crystallites. Hardness of weld metal is not high and amounts, on average, to *HV* 1300 – 1700 MPa (Figure 4). The structure of HAZ metal at the overheating region is ferritic-pearlitic with thin ferrite fringes at the boundaries of former austenitic grains (index 6). Sometimes grains of 5 and 7 indices are observed. In some regions in the weld height the overheating (coarse-grained) zone is absent. Metal hardness at the overheating region is *HV* 1200 – 1500 MPa.

The fine-grained region is available in all the samples, the ferritic grain index corresponds to 9. The structure of the fine-grained region is ferritic-pearlitic with hardness *HV* 1100 – 1400 MPa.

Examination of samples after welding in PPM (Figure 4) showed that the structure of the weld metal is fine-dispersed ferritic pearlitic with a precipitation of a hypoeutectic ferrite along the boundaries of crystallites, thus providing higher hardness *HV* 1600 – 2300 MPa as compared with that in CM. Sometimes, small bainitic regions are observed with hardness *HV* 2500 – 2610 MPa that is not observed in welding in CM.

HAZ metal structure in welding with a pulsed-periodic radiation is differed from that in case of welding with a continuous radiation by almost complete absence of clearly expressed region of overheating (coarse-grained zone). In HAZ region, adjacent to the weld, the grain index is 5 – 6, the structure is fine-dispersed ferritic-pearlitic with a precipitation of a hypoeutectic ferrite along the boundaries of the former austenitic grains. Hardness of this region is *HV* 1350 – 1600 MPa. In welding with a continuous radiation the structure of HAZ metal, not adjacent to the weld, is similar to the that of the fine-grained region.

CONCLUSIONS

1. PPM modulation of CO_2-laser radiation makes it possible to produce more narrow and deep welds than CM, when $P_{pulse} = P_{cont}$. Penetration depth is increased by 20 – 50 % and the weld shape factor is decreased by 20 – 25 %.

2. Position of optimum for a pulse duty factor and frequency of pulses depends on the radiation power and welding speed. With a growth of the average radiation power in a pulse the optimum pulse duty factor is increased and the optimum frequency is decreased. Increase in welding speed leads to the decrease in the optimum pulse duty factor.

3. In welding low-carbon steels in PPM the HAZ width is decreased. Region of overheating (coarse-grained) is either absent or becomes not clearly defined. With decrease in thickness of sheet metal welded the clearly defined regions of overheating are sometimes observed. In all the cases the significant increase in hardness was not observed in the coarse-grained regions unlike the traditional methods of welding.

4. In welding in PPM the regions of a bainitic structure were observed in weld metal. This strong ductile structure favours increase in hardness and strength of weld and HAZ metal that is an advantage as compared with welding in CM.

5. Grain index (characteristic of structure dispersity) in welding with both types of radiation of CO_2-laser is almost similar. It is similar to the grain index in laser welding at ≈ 60 m/h speed [7], that indicates the energy input typical of the medium-speed laser welding.

6. Results of tensile tests showed that metal of welds made by the laser welding in CM is equal in strength to the parent metal (steel 08rm, 10rm, 15rm). Strength of penetrations and butt joints welded in PPM is by 5 – 15 % higher than that of similar joints made at the same power and speed in CM.

REFERENCES

1. Zhuravlyov, V.N., Nikolaeva, O.I. (1981) *Machine-building steels*. Handbook. Moscow: Mashinostroyeniye.
2. (1974) *Technology of electric welding of metals alloys by fusion*. Ed. by B.E. Paton. Moscow: Mashinostroyeniye.
3. Grigoriants, A.G., Shiganov, I.N. (1988) Laser technology and technique. In: *Laser welding of metals.* Moscow: Vysshaya Shkola.
4. Basov, N.G., Bashenko, V.V., Gorny, S.G. *et al*. (1985) Physical-technological peculiarities of laser welding in continuous and pulsed-periodic modes. *Svarochnoye Proizvodstvo*, **8**, 2 – 3.
5. Abilsiitov, G.A., Golubev, V.S., Gontar, V.G. *et al*. (1991) *Technological lasers*. Handbook. Moscow: Mashinostroyeniye.
6. Garashchuk, V.P., Shelyagin, V.D., Nazarenko, O.K. *et al*. (1997) Technological CO_2-laser LT-4 of 10 kW capacity. *Avtomaticheskaya Svarka*, **1**, 36 – 39.
7. Rybakov, A.A., Yakubovsky, V.V., Kirian, V.I. *et al*. (1995) Investigation of performance of welded joints of pipe steel 10G2BT made by two-pass laser welding. *Ibid*., **7**, 12 – 17.